SYNTHESIS AND PROTON CONDUCTIVITY STUDIES OF AZOLE-MODIFIED POLY(GLYCIDYL METHACRYLATE)

by

Sevim ÜNÜGÜR ÇELİK

January 2008

SYNTHESIS AND PROTON CONDUCTIVITY STUDIES OF AZOLE-MODIFIED POLY(GLYCIDYL METHACRYLATE)

by

Sevim ÜNÜGÜR ÇELİK

A thesis submitted to

the Graduate Institute of Science and Engineering

of

Fatih University

is partial fulfillment of the requirements for the degree of

Master of Science

in

Chemistry

January 2008
Istanbul, Turkey

APPROVAL PAGE

I certify that this thesis satisfies all the requirements as a thesis for the degree of Master of Science.

_____

Assist. Prof. Dr. Metin TÜLÜ
Head of Department

This is to certify that I have read this thesis and that in my opinion it is fully adequate, in scope and quality, as a thesis for the degree of Master of Science.

_____

Assoc. Prof. Dr. Ayhan BOZKURT
Supervisor

Examining Committee Members

Assoc. Prof. Dr. Ayhan BOZKURT   _____

Assoc. Prof. Dr. Ali ATA   _____

Assist. Prof. Dr. Ali Ekrem MÜFTÜOĞLU   _____

It is approved that this thesis has been written in compliance with the formatting rules laid down by the Graduate Institute of Sciences and Engineering.

_____

Assist. Prof. Dr. Nurullah ARSLAN

Director

January 2008

SYNTHESIS AND PROTON CONDUCTIVITY STUDIES OF AZOLE-MODIFIED POLY(GLYCIDYL METHACRYLATE)

Sevim Ünügür Çelik

M.Sc. Thesis – Chemistry
January 2008

Supervisor: Assoc. Prof. Dr. Ayhan BOZKURT

ABSTRACT

High temperature tolerant proton conducting membranes have become crucial for high efficiency during their application in clean energy resources such as polymer electrolyte membrane fuel cells (PEMFC). In this study, 1,2,4-triazole and 5-aminotetrazole functional poly(glycidyl methacrylate) polymers have been synthesized and their anhydrous proton conducting properties were investigated after doping with trifloromethane sulfonic acid (triflic acid) and phosphoric acid. Poly(glycidyl methacrylate) (PGMA) was prepared by conventional solution polymerization and then modified with 1H-1,2,4-triazole, 3-Amino-1,2,4-triazole and 5-aminotetrazole via ring opening of the epoxide ring. The FT-IR, solid state ^{13}C CP-MAS NMR and elemental analysis studies verify the high immobilization of the azoles into the polymer chain. Phosphoric acid doped polymers showed lower Tg values and higher proton conductivities. TGA analysis showed thermal stability of the polymer electrolytes up to at least 200 ^{o}C. PGMATri4H$_3$PO$_4$ and PGMAATet4H$_3$PO$_4$ showed a maximum water-free proton conductivity of approximately 0.01 S/cm at 150 ^{0}C and that of PGMAATri2H$_3$PO$_4$ was 1 x 10^{-3} S/cm at 150 ^{0}C.

Keywords: Poly (glycidyl methacrylate), 1H-1,2,4-triazole, 3-amino-1,2,4-triazole, 5-aminotetrazole, polymer electrolyte, anhydrous proton conductivity.

AZOL FONKSİYONLU POLİ(GLİSİDİL METAKRİLAT) SENTEZİ VE PROTON İLETKENLİK ÇALIŞMASI

Sevim Ünügür Çelik

Yüksek Lisans Tezi – Kimya
Ocak 2008

Tez Yöneticisi: Doç. Dr. Ayhan BOZKURT

ÖZ

Polimer elektrolit membranlı yakıt pilleri (PEMFC) gibi temiz enerji kaynaklarında kullanıldığında yüksek verim elde etmek için yüksek sıcaklığa dayanıklı proton iletken membran geliştirilmesi önemli hale gelmiştir. Bu çalışmada, 1,2,4-triazol ve 5-aminotetrazol fonksiyonlu poli(glisidil metakrilat) polymerleri sentezlenmiştir ve triflorometane sulfonik asit (triflik asit) ve fosforik asit ile dop edildikten sonra nemsiz proton iletkenlik özellikleri incelenmiştir. Poli(glisidil metakrilat) (PGMA) serbest radikal polimerizasyonu ile üretilmiş ve sonra epoksi halkası açılarak 1H-1,2,4-triazol, 3-Amino-1,2,4-triazol ve 5-aminotetrazol ile modifiye edilmiştir. FT-IR, katı hal ^{13}C CP-MAS NMR ve elemental analiz çalışmaları azole gruplarının polimer zincirine yüksek oranda immobilize edildiğini doğrulamaktadır. Fosforik asit dope edilen polimerler daha düşük Tg ve daha yüksek proton iletkenliğe sahipler. TGA analizi polimer elektrolitlerin en az 200 ^{o}C'ye kadar termal kararlılığa sahip olduklarını gösterdi. PGMATri4H$_3$PO$_4$ ve PGMAATet4H$_3$PO$_4$ nümunelerinin maksimum nemsiz proton iletkenlikleri yaklaşık 150 ^{0}C'de 0.01 S/cm ve PGMAATri2H$_3$PO$_4$ nümunesininki de aynı sıcaklıkta 1 x 10^{-3} S/cm'dir.

Anahtar Kelimeler: Poli (glisidil metakrilat), 1H-1,2,4-triazol, 3-amino-1,2,4-triazol, 5-aminotetrazol, polimer elektrolit, nemsiz proton iletkenlik.

ACKNOWLEDGEMENTS

TABLE OF CONTENTS

LIST OF TABLES

TABLE

LIST OF FIGURES

FIGURE

LIST OF SYMBOLS AND ABBREVATIONS

SYMBOLS/ABBREVATIONS

PGMA	Poly(glycidyl methacrylate)
Tri	1H-1,2,4-triazole
ATri	3-amino-1,2,4-triazole
ATet	5-aminotetrazole
TA	Trifluoromethanesulfonic acid
PVPA	Poly(vinylphosphonic acid)
PAMPSA	Poly(2-acrylamido-2-methyl -1-propanesulfonic acid)
PEM	Proton Exchange Membrane
PEMFC	Proton Exchange Membrane Fuel Cell
PTFE	Poly(tetraflouroethylene)
PBI	Polybenzimidazole
PEO	Poly(ethylene oxide)
PEI	Poly(ethyleneimine)
PAAM	Poly(acrylamide)
PAA	Polyacrylic Acid
MDP	Mono-dodecylphosphate
MP	Methanediphosphonic Acid
AFC	Alkaline Fuel Cell
PAFC	Phosphoric Acid Fuel Cell
MCFC	Molten Carbonate Fuel Cell
ITSOFC	Intermediate Temperature Solid Oxide Fuel Cell
TSOFC	Tubular Solid Oxide Fuel Cell
VTF	Vogel-Tammann-Fulcher

CHAPTER 1

INTRODUCTION

Recently, operation of PEMFCs at intermediate temperature, particularly between 100-200°C has been considered to provide several advantages such as improved carbon monoxide tolerance, higher energy efficiency, and simplified heat managements (Ianniello et al., 1994, Antonucci et al., 1999). In this context, anhydrous polymer electrolyte membranes are considered as alternative materials that have almost no dependence on humidity and can maintain high proton conductivity (~ 0.01 S/cm) at higher temperatures.

It has been shown that replacement of water by heterocycles, such as imidazole, pyrazole or benzimidazole leads to proton conductivities at temperatures above 100 ^{o}C (Kreuer et al., 1998). These heterocycles form hydrogen bonded networks and proton transport occurs by hop-turn mechanism via structure diffusion. Although these proton solvents are widely used in closed electrochemical cells, such as supercapacitators and electrochemical devices, the volatility of the heterocycles prevents them from being used in open electrochemical systems, such as fuel cells. Therefore, the use of heterocycles as the proton solvent requires their immobilisation in the polymer membrane in such a way that high mobility of the protonic charge carriers is still provided (Kreuer, 2001).

As a first attempt towards a full immobilization of imidazole as proton solvent Schuster et al. prepared imidazole terminated short oligo-ethyleneoxide (EO) chains (Schuster et al., 2001). They obtained a maximum conductivity of $5x10^{-3}$ S/cm at 120 ^{o}C for the trifilic acid doped samples. Later, Herz et al. prepared fully polymeric solvents with high proton mobility by tethering imidazole and benzimidazole units into polystyrene and siloxane network, respectively (Herz et al., 2003). They obtained a maximum conductivity of $7x10^{-4}$ S/cm at 200 ^{o}C. Scharfenberger et al. synthesized

imidazole functional cyclic oligomeric siloxane and polysiloxane obtaining highest conductivity of 10^{-3} S/cm and 5×10^{-4} S/cm, respectively (Scharfenberger et al., 2006).

While the high proton mobility has been observed in imidazole-based materials, including ionic liquids, oligomers and polymers, the electrochemical stability of imidazole appears to be inadequate for fuel cell applications because of the high electronic density of imidazole ring (Noda et al., 2003, Yang et al., 2001, Deng et al., 2004).

1H-1,2,4-triazole is another promising heterocycle whose molecular structure is similar to imidazole and therefore may conduct protons via structure diffusion mechanism. Compared with imidazole (T_{mp} 89 ^{o}C, T_{bp} 257 ^{o}C), 1H-1,2,4-triazole has a higher melting point (120 ^{o}C) and a similar boiling point (256 ^{o}C) owing to its strong hydrogen bonds. The proton conductivity of pure 1H-1,2,4-triazole is 1.5 $\times 10^{-4}$ S/cm at 115 ^{o}C and 1.2 $\times 10^{-3}$ S/cm at melting point 120 ^{o}C. This result proves that self dissociation of 1H-1,2,4-triazole produces highly mobile proton charge carriers (Li et al., 2005).

In this work, poly (glycidyl methacrylate), PGMA was produced by free radical polymerization of glycidyl methacrylate. Then, 1H-1,2,4-triazole, 3-amino-1,2,4-triazole and 5-aminotetrazole were tethered into the PGMA via ring opening of the epoxide group. The materials were doped with triflic acid and phosphoric acid at several stoichiometric ratios and effect of dopant in proton conductivity was studied via impedance spectrometer.

CHAPTER 2

FUEL CELLS

Fuel cells are electrochemical devices that convert the chemical energy of a reaction directly into electrical energy. The basic physical structure or building block of a fuel cell consists of an electrolyte layer in contact with a porous anode and cathode on either side. A schematic representation of a fuel cell with the reactant/product gases and the ion conduction flow directions through the cell is shown in Fig. 2.1.

Anode: H_2 $\rightarrow$ $2H^+ + 2e^-$

Cathode: $\frac{1}{2} O_2 + 2H^+ + 2e^-$ $\rightarrow$ H_2O

Overall reaction: $H_2 + \frac{1}{2} O_2$ $\rightarrow$ H_2O
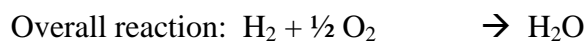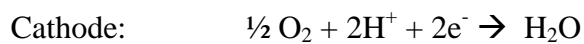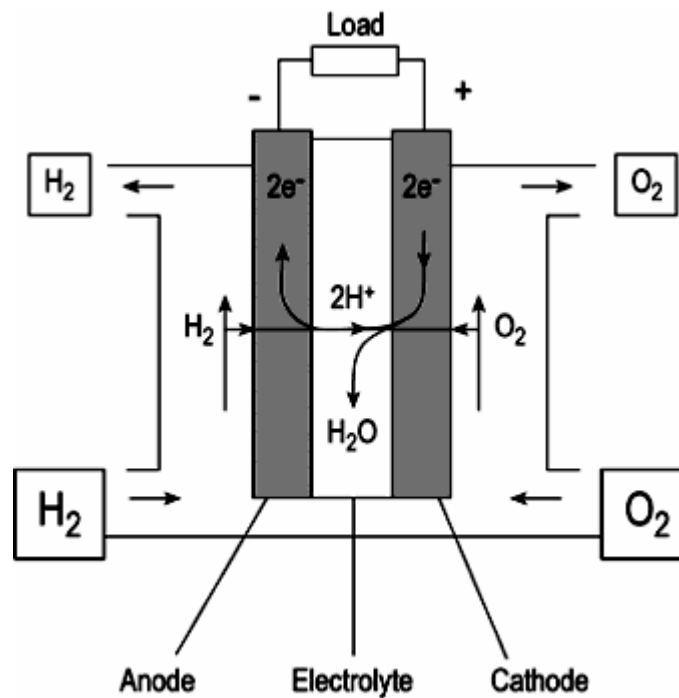
Figure 2.1 Schematic illustration of an individual fuel cell (Cremers and Stimming, 2004)

In a typical fuel cell, gaseous fuels are fed continuously to the anode (negative electrode) compartment and an oxidant (i.e., oxygen from air) is fed continuously to the cathode (positive electrode) compartment; the electrochemical reactions take place at the electrodes to produce an electric current. A fuel cell, although having components and characteristics similar to those of a typical battery, differs in several respects. The battery is an energy storage device. The maximum energy available is determined by the amount of chemical reactant stored within the battery itself. The battery will cease to produce electrical energy when the chemical reactants are consumed (i.e., discharged). In a secondary battery, the reactants are regenerated by recharging, which involves putting energy into the battery from an external source. The fuel cell, on the other hand, is an energy conversion device that theoretically has the capability of producing electrical energy for as long as the fuel and oxidant are supplied to the electrodes. Fig. 2.1 is a simplified diagram that demonstrates how the fuel cell works. In reality, degradation, primarily corrosion, or malfunction of components limits the practical operating life of fuel cells. Note that the ion specie and its transport direction can differ, influencing the site of water production and removal, a system impact. The ion can be either a positive or a negative ion, meaning that the ion carries either a positive or negative charge (surplus or deficit of electrons). The fuel or oxidant gases flow past the surface of the anode or cathode opposite the electrolyte and generate electrical energy by the electrochemical oxidation of fuel, usually hydrogen, and the electrochemical reduction of the oxidant, usually oxygen (Fuel Cell Handbook, 2000).

A variety of fuel cells are in different stages of development. They can be classified by use of diverse categories, depending on the combination of type of fuel and oxidant, whether the fuel is processed outside (external reforming) or inside (internal reforming) the fuel cell, the type of electrolyte, the temperature of operation, whether the reactants are fed to the cell by internal or external manifolds, etc. The most common classification of fuel cells is by the type of electrolyte used in the cells and includes 1) polymer electrolyte fuel cell (PEFC), 2) alkaline fuel cell (AFC), 3) phosphoric acid fuel cell (PAFC), 4) molten carbonate fuel cell (MCFC), 5) intermediate temperature solid oxide fuel cell (ITSOFC), and 6) tubular solid oxide fuel cell (TSOFC). These fuel cells are listed in the order of approximate operating temperature, ranging from ~80 ^{o}C for PEFC, ~100 ^{o}C for AFC, ~200 ^{o}C for PAFC, ~650 ^{o}C for MCFC, ~800 ^{o}C for ITSOFC, and 1000 ^{o}C for TSOFC. The operating temperature and useful life of a fuel

cell dictate the physicochemical and thermomechanical properties of materials used in the cell components (i.e., electrodes, electrolyte, interconnect, current collector, etc.). Aqueous electrolytes are limited to temperatures of about 200 ^{o}C or lower because of their high water vapor pressure and/or rapid degradation at higher temperatures. The operating temperature also plays an important role in dictating the type of fuel that can be used in a fuel cell. The low-temperature fuel cells with aqueous electrolytes are, in most practical applications, restricted to hydrogen as a fuel. In high-temperature fuel cells, CO and even CH_4 can be used because of the inherently rapid electrode kinetics and the lesser need for high catalytic activity at high temperature. However, descriptions later in this section note that the higher temperature cells can favor the conversion of CO and CH_4 to hydrogen, then use the equivalent hydrogen as the actual fuel (Fuel Cell Handbook, 2000).

2.1 Polymer Electrolyte Fuel Cell (PEFC)

The electrolyte in this fuel cell is an ion exchange membrane (fluorinated sulfonic acid polymer or other similar polymer) that is an excellent proton conductor. The only liquid in this fuel cell is water; thus, corrosion problems are minimal. Water management in the membrane is critical for efficient performance; the fuel cell must operate under conditions where the byproduct water does not evaporate faster than it is produced because the membrane must be hydrated. Because of the limitation on the operating1-4 temperature imposed by the polymer, usually less than 120 ^{o}C, and because of problems with water balance, a H_2-rich gas with minimal or no CO (a poison at low temperature) is used. Higher catalyst loading (Pt in most cases) than that used in PAFCs is required for both the anode and cathode (Fuel Cell Handbook, 2000).

2.2 Alkaline Fuel Cell (AFC)

The electrolyte in this fuel cell is concentrated (85 wt%) KOH in fuel cells operated at high temperature (~250 ^{o}C), or less concentrated (35-50 wt%) KOH for lower temperature (<120 ^{o}C) operation. The electrolyte is retained in a matrix (usually asbestos), and a wide range of electrocatalysts can be used (e.g., Ni, Ag, metal oxides, spinels, and noble metals). The fuel supply is limited to non-reactive constituents except for hydrogen. CO is a poison, and CO_2 will react with the KOH to form K_2CO_3, thus

altering the electrolyte. Even the small amount of CO_2 in air must be considered with the alkaline cell (Fuel Cell Handbook, 2000).

2.3 Phosphoric Acid Fuel Cell (PAFC)

Phosphoric acid concentrated to 100 % is used for the electrolyte in this fuel cell, which operates at 150 to 220 ^{o}C. At lower temperatures, phosphoric acid is a poor ionic conductor, and CO poisoning of the Pt electrocatalyst in the anode becomes severe. The relative stability of concentrated phosphoric acid is high compared to other common acids; consequently the PAFC is capable of operating at the high end of the acid temperature range (100 to 220 ^{o}C). In addition, the use of concentrated acid (100 %) minimizes the water vapor pressure so water management in the cell is not difficult. The matrix universally used to retain the acid is silicon carbide, and the electrocatalyst in both the anode and cathode is Pt (Fuel Cell Handbook, 2000).

2.4 Molten Carbonate Fuel Cell (MCFC)

The electrolyte in this fuel cell is usually a combination of alkali carbonates, which is retained in a ceramic matrix of $LiAlO_2$. The fuel cell operates at 600 to 700 ^{o}C where the alkali carbonates form a highly conductive molten salt, with carbonate ions providing ionic conduction. At the high operating temperatures in MCFCs, Ni (anode) and nickel oxide (cathode) are adequate to promote reaction. Noble metals are not required (Fuel Cell Handbook, 2000).

2.5 Intermediate Temperature Solid Oxide Fuel Cell (ITSOFC)

The electrolyte and electrode materials in this fuel cell are basically the same as used in the TSOFC. The ITSOFC operates at a lower temperature, however, typically between 600 to 800 ^{o}C. For this reason, thin film technology is being developed to promote ionic conduction; alternative electrolyte materials are also being developed (Fuel Cell Handbook, 2000).

2.6 Tubular Solid Oxide Fuel Cell (TSOFC)

The electrolyte in this fuel cell is a solid, nonporous metal oxide, usually Y_2O_3-stabilized ZrO_2. The cell operates at 1000 ^{o}C where ionic conduction by oxygen ions takes place. Typically, the anode is $Co-ZrO_2$ or $Ni-ZrO_2$ cermet, and the cathode is Sr-doped $LaMnO_3$. In low-temperature fuel cells (PEFC, AFC, PAFC), protons or hydroxyl ions are the major charge carriers in the electrolyte, whereas in the high-temperature fuel cells, MCFC, ITSOFC, and TSOFC, carbonate ions and oxygen ions are the charge carriers, respectively. Major differences between the various cells are shown in Table 2.1 (Fuel Cell Handbook, 2000).

Table 2.1 Summary of major differences of the fuel cell types (Fuel Cell Handbook, 2000).

	PEFC	AFC	PAFC	MCFC	ITSOFC	TSOFC
Electrolyte	Ion Exchange Membranes	Mobilized or Immobilized Potassium Hydroxide	Immobilized Liquid Phosphoric Acid	Immobilized Liquid Molten Carbonate	Ceramic	Ceramic
Operating Temperature	80°C	65-220°C	205°C	650°C	600-800°C	800-1000°C
Charge Carrier	H^+	OH^-	H^+	CO_3^{2-}	O^{2-}	O^{2-}
External Reformer for CH_4 (below)	Yes	Yes	Yes	No	No	No
Prime Cell Components	Carbon-based	Carbon-based	Graphite-based	Stainless-based	Ceramic	Ceramic
Catalyst	Platinum	Platinum	Platinum	Nickel	Perovskites	Perovskites
Product Water Management	Evaporative	Evaporative	Evaporative	Gaseous Product	Gaseous Product	Gaseous Product
Product Heat Management	Process Gas + Independent Cooling Medium	Process Gas + Electrolyte Calculation	Process Gas + Independent Cooling Medium	Internal Reforming + Process Gas	Internal Reforming + Process Gas	Internal Reforming + Process Gas

CHAPTER 3

PROTON CONDUCTION MECHANISMS

A proton conductor is an electrolyte, typically a solid electrolyte, in which movable hydrogen ions (protons) are the primary charge carriers. Proton conductors are usually composed of polymer or ceramic because the pore size is small enough that larger negative ions are locked into the solid matrix, and only very small ions (positive hydrogen ions — bare protons) can participate in a direct current. Proton conductors are usually solid materials. When in the form of thin membranes, proton conductors are an essential part of small, inexpensive fuel cells.

Proton conduction was first suggested by Alfred Rene Jean Paul Ubbelohde (14 December 1907 - 7 January 1988) and S.E. Rogers. Water is the best solvent for protons and exhibits unusually high equivalent conductivity of protons, which exceeds the hydrodynamic limit by a factor of 4.5 under ambient conditions. The process for proton transport in water is explained by "Grotthuss mechanism" (Grotthuss, 1806, Kreuer, 1997) also called "hopping mechanism" or "chain mechanism" or "structure diffusion". The proton transport comprises rapid intermolecular proton transfers (Hopping) down a chain of hydrogen bonds where the transfer events are assumed to be highly correlated, and reorientation of water dipoles in order to produce a configuration which allows for the next hopping event (Grotthuss, 1806, Kreuer, 1997).
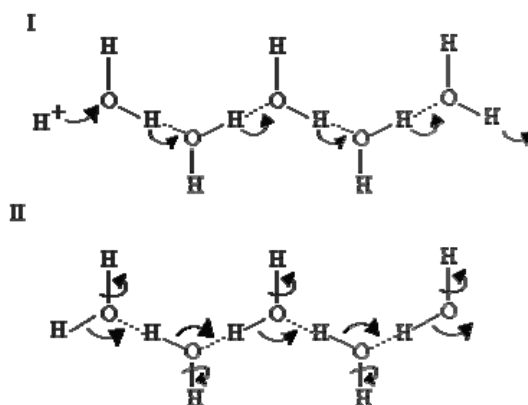
Figure 3.1 Grotthuss mechanism (Crofts, 1996).

The first process leads to a polarization of the hydrogen bond chain, i.e. to a local relative charge displacement, but not to dc conductivity. The second process causes the depolarization of the chain by reorientation of the water dipoles (Fig. 3.1). The mechanism of proton migration in water has been studied extensively (Eigen, 1964, Agmon, 1995, Agmon, 1996). Basically, for a fast Grotthusstype mechanism, it must enable the formation of protonic defects and provide strongly fluctuating proton donor and acceptor functions in an otherwise non-polar environment. The latter avoids strong solvent effects that tend to suppress proton transfer reactions (Kreuer, 1997, Kreuer , 1996). However, this mechanism cannot explain all abnormal proton conductive systems. Based on NMR spectra and self-diffusion coefficients, Kreuer et al. (Kreuer et al., 1982) proposed "Vehicle mechanism", also called molecular diffusion, for the interpretation of the conductivity of fast proton conductors such as zeolites, Nafion etc. According to this model the proton does not migrate as H^+ but as H_3O^+, NH_4^+, etc., bonded to a " vehicle" such as H_2O, NH_3, etc. (Fig. 3.2) The "unloaded" vehicles move in the opposite direction. Hydrogen bond is not necessary for proton transport with this model.

Grotthuss Mechanism

Vehicle Mechanism
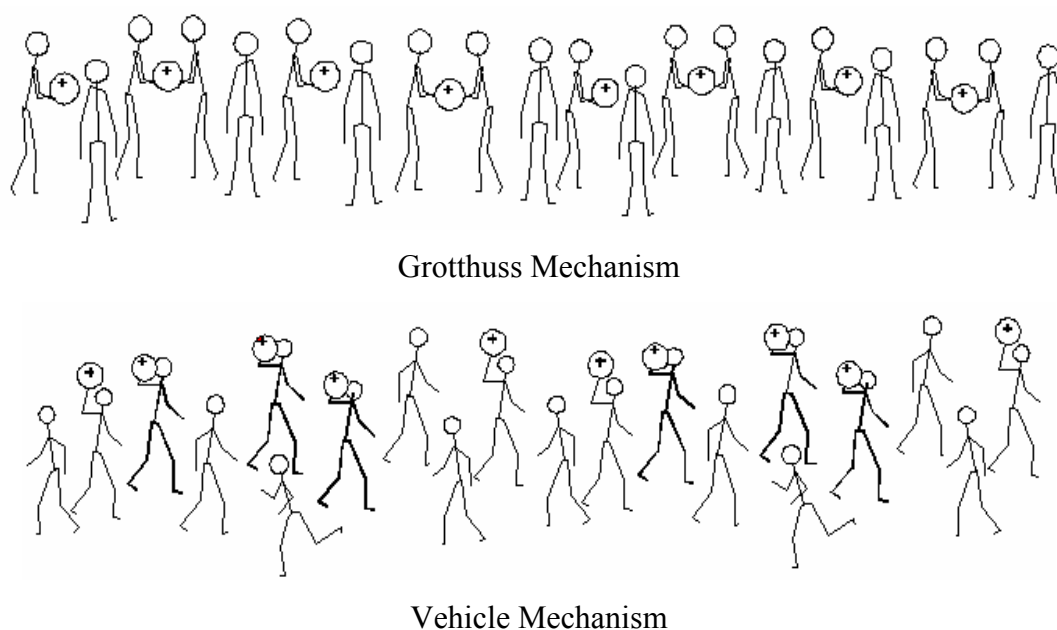
Figure 3.2 Schematic representation of phenomena involved in proton conduction mechanisms (Kreuer et al., 1982).

In some systems, the conduction mechanism is contributed by these two models together. Also, the conduction mechanism can change from one model to another model based on the temperature and concentration of the system. For example, in concentrated aqueous solutions of acids such as aqueous HCl, the proton conduction can be well explained by vehicle mechanism. However, if the acid solutions are diluted, i.e. increasing solvent (H_2O) concentration, there is an increasing contribution of structure diffusion to the overall conductivity, i.e. both of the mechanisms (the mixed mechanism) exist for proton conduction. (Kreuer et al., 1992). Kreuer distinguished the molecular diffusion (vehicle mechanism) and structure diffusion (Grotthuss mechanism) of proton by measuring the self-diffusion coefficients by means of the PFG-NMR technique. (Kreuer, 1996, Kreuer et al., 1992, Dippel and Kreuer, 1991, Bozkurt et al., 1999). Basically, in anhydrous oxo-acids such as H_3PO_4 (Dippel et al., 1993) solid acidic salts of oxo-acids such as $CsHSO_4$ (Cuddeback et al., 1953) and $Zr(HPO_4)_2$ (Alberti et al., 1984) or oxo-acid/polymer blends such as $BPEI/0.5H_2SO_4$ (Lassegues et al., 1989), the proton conductivity can be entirely explained by structure diffusion. In hydrated acidic polymers such as Nafion (Slade et al., 1983), proton conductivity is controlled by molecular diffusion. However, the boiling point of water limits the usage

of water as a proton solvent at high temperature. H_3PO_4, due to the formation of 3D polyphosphoric acid network for proton transport at high temperatures and anhydrous environment, is the best solvent for proton at high temperatures and anhydrous conditions. It has been demonstrated that in highly viscous anhydrous phosphoric acid, 98% of the total conductivity arises from structure diffusion of proton (Dippel et al., 1993). Recently, Kreuer (Kreuer et al., 1998) proposed that imidazole, benzimidazole and pyrazole could conduct proton as water does when ionized. After Kreuer's work, a series of work has been done with imidazole of benzimidazole as proton conductor (Ma, 2004).

Phosphoric acid, which can form 3-D hydrogen bonding network due to its special structure, is a very good proton conductive medium. The super-cooled melted pure acid has a conductivity of 0.053 S/cm at 30oC, and this high value is known to come from the extensive self-ionization of H_3PO_4 (Greenwood and Thompson, 1959, Munson, 1964). Structure diffusion was proposed as the operating fast conduction and diffusion mechanism in fused phosphoric acid, where the transference number of proton is close to 1 (≈0.975) (Dippel et al., 1993). Addition of water increases the dissociation, decreases the viscosity therefore brings the conductivity to a maximum of 0.27 S/cm for 45 % acid by weight (Chin and Chang, 1989). Further dilution decreases the number of charge carriers more rapidly than the viscosity, and the conductivity drops finally to the value of pure water. Phosphoric acid can be regarded as a mixture of P_2O_5 and H_2O. At high temperatures, phosphoric acid undergoes auto-dehydration process in addition to the self-dissociation process. The dehydration is reversible at low temperatures if water is provided. Therefore, phosphoric acid can conduct proton at high temperatures and very low relative humidity by forming polyphosphoric acid network.

It is well known that proton conducing polymer electrolyte can be obtained by doping polymers bearing basic groups such as ether, alcohol, imine, amide or imide with strong acids such as H_3PO_4 or H_2SO_4. H_2SO_4 is more acidic and oxidative than H_3PO_4 and tends to form a salt with a basic site in the polymer thus decreases the concentration of the proton charge carrier. Moreover, the thermal stability of a H_2SO_4 doped polymer is not good due to its oxidizing property. H_3PO_4 is a relatively weak acid. It interacts with the polymer through hydrogen bond or proton transfer reaction depending on the basicity of the polymer.

In acid/polymer systems, the polymer has two functions: on one hand, it has to be sufficiently basic to dissolve and complex with the acid, i.e. it acts as a solvent in which the acid undergoes some dissociation. On the other hand, excess acid is usually needed to obtain a high conductivity. Thus the polymer acts as a matrix to retain the excess acid. However, most of these materials suffer from fundamental limitations such as insufficient chemical stability (e.g. hydrolysis of ethers or amides) or low mechanical stability, especially at higher temperatures or with excess acid. Films with good thermal and mechanical stabilities for high temperature application can be obtained from polymers with high glass transition temperatures such as polybenzimidazole. However, the segmental movement of polymer can assist the proton conductivity so that flexible polymers with low glass transition temperatures are preferred (Ma, 2004).

CHAPTER 4

POLYMER MEMBRANES

4.1 HYDRATED PROTON CONDUCTING MEMBRANES

In general, proton-conducting polymers are usually based on polymer electrolytes, which have negatively charged groups attached to the polymer backbone. These polymer electrolytes tend to be rather rigid and are poor proton conductors unless water is absorbed. The proton conductivity of hydrated polymer electrolytes dramatically increases with water content and reaches values of 10^{-2}-10^{-1} S cm^{-1}.

The first PEFC used in an operational system was the GE-built 1 kW Gemini power plant (Zawodzinski et al., 1993). This system was used as the primary power source for the Gemini spacecraft during the mid-1960s. The performances and lifetimes of the Gemini PEFCs were limited due to the degradation of poly(styrene sulfonic acid) membrane employed at that time. The degradation mechanism determined by GE was generally accepted until the present time. It was postulated that HO$_2$ radicals attack the polymer electrolyte membrane. The second GE PEFC unit was a 350 W module that powered the Biosatellite spacecraft in 1969. An improved Nafion$^®$ membrane manufactured by DuPont was used as the electrolyte. Fig. 4.1 shows the chemical structures of Nafion$^®$ and other perfuorinated electrolyte membranes. The performance and lifetime of PEFCs have significantly improved since Nafion$^®$ was developed in 1968. Lifetimes of over 50,000 h have been achieved with commercial Nafion$^®$ 120 (Rikukawa and Sanui, 2000).
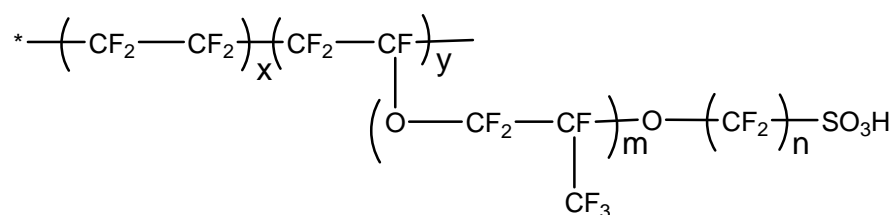
Nafion 117	m≥1, n=2, x=5-13.5, y=1000
Flemion	m=0, n=1-5
Aciplex	m=0, n=2-5, x=1.5-14
Dow membrane	m=0, n=2, x=3.6-10

Figure 4.1 Chemical structures of perfluorinated polymer electrolyte membranes (Rikukawa and Sanui, 2000).

As seen in Fig. 4.2, the Yeager Three Phase Model is a phenomenological based model. This model is based on a three-phase clustered system with interconnecting channels within the polymer. The three regions consist of (A) a fluorocarbon backbone, some of which is microcrystalline, (B) an interfacial region of relatively large fractional void volume containing some pendant side chains, some water, and those sulfate or carboxylic groups and counter ions which are not in clusters, and (C) the clustered regions where the majority of the ionic exchange sites, counter ions, and sorbed water exists (Yeager and Eisenberg, 1982; Brookman and Nicholson, 1986).

From experimental means, such as, small-angle x-ray scattering (SAXS) it has been determined that the phase-separated morphology is on the order of 30-50Å Bragg spacing. However, upon hydration, Nafion® with its unique ability to sorb relatively large amounts of water, can increase its dry weight by as much as 50 percent or more depending upon equivalent weight, counter ion, and temperature. Upon hydration, however, cluster diameter and the number of exchange sites are thought to increase, leading to fewer, larger clusters.
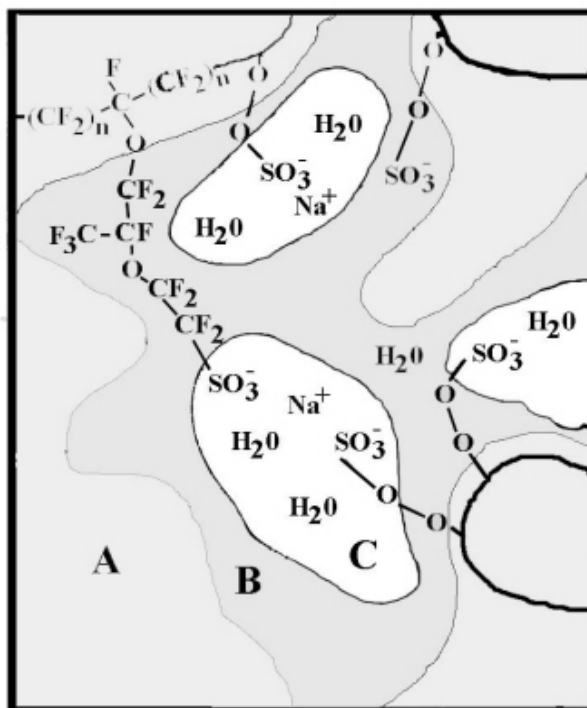
Figure 4.2 The Yeager 3 Phase Model of Nafion® Clusters (Yeager and Eisenberg, 1982).

Nafion® 117 and 115 have equivalent repeat unit molecular weights of 1100 and thicknesses in the dry state of 175 and 125 μm, respectively. Nafion® 120 has an equivalent weight of 1200 and a dry state thickness of 260 μm. Ballard Technologies Corporation showed the possibility of the application of PEFC for electric vehicles by using experimental perfuorinated membranes developed by Dow Chemical. Development of PEFC has been accelerated year by year after the report of Ballard Technologies Corporation. The Dow membrane has an equivalent weight of approximately 800 and a thickness in the wet state of 125 mm. In addition, Flemion® R, S, T, which have equivalent repeat unit molecular weights of 1000 and dry state thicknesses of 50, 80, 120 μm, respectively, were also developed by Asahi Glass Company (Watkins et al., 1993). Asahi Chemical Industry manufactured a series of Aciplex®-S membranes, which have equivalent repeat unit molecular weights of 1000-1200 and dry state thicknesses of 25-100 μm.

These perfuorinated ion exchange membranes including Neosepta-Fw (Tokuyama) and Gore-Selectw (W. L. Gore and Associates, Inc.) have been developed for chlor-alkali electrolysis. The water uptake and proton transport properties of this

type of membrane have signifcant effects on the performance of PEFCs. These membranes have water uptakes of above 15 H_2O/-SO_3H, and maximizing membrane water uptake also maximizes the proton conductivity. In general, conductivities can reach values of 10^{-2}-10^{-1} S cm^{-1}. All of these membranes possess good thermal, chemical, and mechanical properties due to their perfuorinated polymer backbones. A limiting factor in PEFCs is the membrane that serves as a structural framework to support the electrodes and transport protons from the anode to the cathode. The limitations to large-scale commercial use include poor ionic conductivities at low humidities and/or elevated temperatures, a susceptibility to chemical degradation at elevated temperatures and finally, membrane cost. These factors can adversely affect fuel cell performance and tend to limit the conditions under which a fuel cell may be operated. For example, the conductivity of Nafion$^®$ reaches up to 10^{-2} S cm^{-1} in its fully hydrated state but dramatically decreases with temperature above the boiling temperature of water because of the loss of absorbed water in the membranes. Consequently, the development of new solid polymer electrolytes, which are cheap materials and possess sufficient electrochemical properties, have become one of the most important areas for research in PEFC and FCEV (Rikukawa and Sanui, 2000).

4.2 ANHYDROUS PROTON CONDUCTIVE MEMBRANES

Proton exchange membrane (PEM) fuel cells have gained prominence after they become applicable to various technological areas particularly on portable power generating systems. In general, polymer based proton conducting materials can be categorized according to the temperature range in which they exhibit high proton conductivity. The first class of materials that can be utilized in the temperature range 25-100°C because their conductivity depends on water content. Within this family of polymers, hydrated perfluorosulfonic acid membranes such as Nafion$^®$, well-established low temperature materials since 1960. These materials are typically phase separated into hydrophilic/hydrophobic domains and conductivity occurs via transport of dissociated protons by the dynamics of water (Kreuer et al., 1993). These hydrated systems have been used as the polymer electrolytes in hydrogen/oxygen polymer electrolyte fuel cells (PEMFCs) due to excellent chemical and mechanical stability as well as high proton conductivity (Rikukawa and Sanui, 2000, Motupally et al., 2000, Costamagna and

Srinivasan, 2001). However, there are several limitations in perfluorosulfonic acid membranes, which retard spread industrial application. The major disadvantages are high cost of the membrane, high operation temperature, high methanol permeability when used in direct methanol fuel cells (DMFCs) and difficult recycling and disposal (Kreuer, 2001, Miyake et al., 2001).

Recently, operation of PEMFCs at intermediate temperature, particularly between 80-180°C has been considered to provide several advantages such as improved carbon monoxide tolerance, higher energy efficiency, and simplified heat managements (Ianniello et al., 1994, Antonucci et al., 1999). In this context, second class of polymer electrolyte membranes are considered as alternative materials that have almost no dependence on humidity and can maintain high proton conductivity (~0.01 S/cm) at medium temperatures. In general, there are three different approaches toward anhydrous PEMs in terms of their chemical structure and conductivity mechanisms:
.

a) Polymer-acid complexes. These are based on polymer networks which contain ether, amide, amine or imino groups are doped with strong acids such as H_3PO_4 or H_2SO_4.

b) Intrinsic proton conductors based on homopolymers, copolymers, and polymer networks produced by tethering the heterocyclic proton solvent.

c) Polymer/heterocycle hybrid electrolytes. In principle, these materials consists of acidic host matrix that forms complexes with amphoteric heterocycles and conduction occurs through protonic defects.

4.2.1 Polymer/Inorganic Acid Complexes

Since 1980's phosphoric acid based polymer electrolytes have received extensive attention due to their applications primarily in fuel cells, as well as electrochromic displays, hydrogen sensors and supercapacitors. The concept is based on the doping of the polymers bearing basic sites with inorganic acids (e.g. H_3PO_4, H_2SO_4). Since pure H_3PO_4 themselves is a good proton conductor because of its extensive self-ionization and low pK_a (Dippel et al., 1993, Munson, 1964). Structure diffusion was proposed as the proton diffusion mechanism in fused phosphoric acid, where the transference number of proton is close to unity (~ 0.975) (Dippel et al., 1993). Phosphoric acid

interacts with polymers through hydrogen bonds depending on the basicity of the polymer and facilitates the formation homogeneous blends. In general, phosphoric acid in polymer electrolytes acts as proton solvent via undergoing some dissociation and plasticizer where segmental movement of polymer assists the proton conductivity. Thus, high conductivity is favored at higher doping levels.

Polymer/acid complexes have usually been prepared by incorporation of acid into the host matrix in a suitable solvent at several stoichiometric ratios. Anhydrous materials have been obtained when the solvent water is removed so that it doesn't involve in proton transfer reactions. A wide variety of materials have already been produced and successfully applied to several electrochemical devices i.e., electrochromic devices, hydrogen sensors and fuel cells (Przyluski and Wieczorek, 1991, Lassegues, 1992, Lassegues et al., 2001, Schuster and Meyer, 2003).

4.2.1.1 PEO x H₃PO₄

Poly(ethyleneoxide), PEO forms well-defined complexes with orthophosphoric acid (Donoso et al., 1988). In the absence of moisture, PEO x H_3PO_4 has a maximum conductivity of $4x10^{-5}$ S/cm at room temperature and $3x10^{-4}$ S/cm at 50 ^{o}C where x is the doping ratio. The temperature dependence of conductivity shows VTF behavior at small doping ratios, indicating the contribution of the segmental relaxations.

4.2.1.2 PEO-PMMA x H₃PO₄

PEO-PMMA host-guest systems were studied by Przyluski et al. (Przyluski et al., 1992, Przyluski et al., 1993). The materials were prepared via thermal polymerization of methyl methacrylate in the presence of PEO at 90 ^{o}C. Maximum conductivity of $2.7x10^{-2}$ S/cm was attained at 50 ^{o}C. PEO-PMMA-H_3PO_4 system was applied to ambient temperature H_2/O_2 fuel cells and the performance was 40 mW/cm^2 under humid conditions.

4.2.1.3 PVA x H₃PO₄

Petty-Week et al. reported on a PVA-H₃PO₄ electrolyte that was blended with a three dimensional interpenetrating network (IPN) formed from methacrylic acid and methylen-bisacrylamide (Petty-Week et al., 1988). PVA-H₃PO₄-IPN was a heterogeneous system where IPN network increased the stiffness of the samples and improved their water insolubility. It was shown that the addition of H₃PO₄ plasticized the material and increased their proton conductivity. The application of PVA-H₃PO₄-IPN (humidified) electrolyte in hydrogen gas sensors (response time < 10 s) was demonstrated (Polak et al., 1986).

4.2.1.4 PEI x Acid

Linear (L) or branched (B) PEI is a water soluble polymer and forms complexes with strong acids such as H_2SO_4, H_3PO_4 and HCl (Daniel et al., 1988a, Schoolman et al., 1992, Tanaka et al., 1995). The interaction between polybase and acid (PEI) was studied FT-IR and Raman spectroscopies. I was confirmed that maximum protonation occurs when x=0.35 (acid concentration with respect to repeat unit of PEI). The proton conductivity of BPEI was found to be higher than LPEI when doped with H_2SO_4, i.e., proton conductivity of LPEI 0.35 H_2SO_4 is ~ 10^{-8} and that of BPEI 0.35 H_2SO_4 is 8.5×10^{-3} S/cm. When the dopant in LPEI was replaced by H_3PO_4, the conductivity was doubled. However, for the BPEI - H_3PO_4 complexes reverse behavior was observed. As the concentration of H_3PO_4 is varied (x= 0.5-2.0), the conductivity of both PEI s reach to their maximum values. The highest proton conductivity of BPEI 2.0 H_3PO_4 is ~ 10^{-3} S/cm at ambient temperature and ~ 10^{-2} S/cm at 100 ^{o}C (Schoolman et al., 1992) and that of LPEI 2.05 H_3PO_4 is 1.4×10^{-3} S/cm at 100 ^{o}C (Tanaka et al., 2000). Schoolman et al. also mentioned the application of BPEI x H_3PO_4 complex electrolytes to electrochromic devices which is designed according to: Glass/ITO/WO₃/BPEIxH₃PO₄/IrO_yH_x/ITO/Glass (Schoolman et al., 1992).

4.2.1.5 PAAM x H₃PO₄

Poly(acrylamide), PAAM is a water soluble polymer that forms homogeneous transparent films when doped with phosphoric acid with a ratio 0.6<x<2 (Rodriguez et

al., 1993). Although the PAAM/H$_3$PO$_4$ showed high room temperature conductivity ~10^{-3} -10^{-2} S/cm (x=2), they were chemically unstable i.e., PAAM in acid crosslinks via intra- and interchain imidization, a process which is accelerated by heating. Although PAAM 1.2 H$_2$SO$_4$ has a highest conductivity within this family of compounds, it hydrolyzes in strong acid solution (Lassegues et al., 1992).

4.2.1.6 Nylon 6-10 x H$_3$PO$_4$

Grondin et al. have investigated several kinds of Nylons (4,6, 6-6, 6-10) and their complex electrolytes with H$_3$PO$_4$ and H$_2$SO$_4$ (Grondin et al., 1995). Nylon 6-10, x H$_3$PO$_4$ (x=0.75 to 2.5) could be processed as thin films on large surfaces. The IR speactra reveal that protonation occurs on the carboxyl group to give C(OH)=NH$^+$. The blends were stable up to 100 ^{o}C under air. The conductivities of Nylon$^®$ and phosphoric acid complexes are close to each other irrespective to type of matrix. Proton conductivity of Nylon 6-10, x H$_3$PO$_4$ (x= 2.-2.5) reached a level of ~ 10^{-4} -10^{-3} S/cm at 25 ^{o}C. Electrochemical stability domain for Nylon/ H$_3$PO$_4$ blends extend over about 1.3 V. The Nylon/H$_2$SO$_4$ blends were chemically unstable and no mechanically stable films could be formed. The properties of some of the described proton polymeric electrolytes are summarized in Table 4.1. It should be emphasized, however, that all of the materials reported were thermally stable up to 100 ^{o}C.

4.2.1.7 PVP x H$_3$PO$_4$

Poly(vinylpyrrolidone), PVP is a thermally stable polymer (decomposition temperature is equal to 380 ^{o}C) and form similar complexes with phosphoric acid. The glass transition temperature (T$_g$) of the pristine polymer is 180 ^{o}C but the H$_3$PO$_4$ acts as plasticizer and shifts the T$_g$ of host matrix to lower temperatures. For example, For PVP 1 H$_3$PO$_4$, the T$_g$ is approximately 100 ^{o}C and for PVP 2 H$_3$PO$_4$ it falls to near 0 ^{o}C (Daniel et al., 1988b). For PVP 1 H$_3$PO$_4$, σ= ~ 10^{-5} S/cm at 130 ^{o}C. For the optimization of the conductivity of PVP-acid complex electrolytes, experiments were carried out using commercially available PVP (M$_w$ =360000). To inhibit high temperature condensations of H$_3$PO$_4$, polyphosphoric acid, PPA was used as dopant. Anhydrous proton conductive PVP x PPA were prepared at various doping ratios (0≤x≤3) (Bozkurt and Meyer, 2001a). FT-IR studies indicated that the interaction between PPA and PVP

occurs not only via carbonyl group but also via protonation of the amide group. TG and IR studies illustrated that polyacid as a dopant improved the decomposition temperature of PVP-*x*-PPA blends to 180 °C. DSC studies show that the T_g of PVP x PPA complexes shifted from 180 °C for x= 0 to -23 °C x=3 due to the plasticizing effect of the polyacid. Maximum threshold conductivity of 1.2x 10^{-3} S/cm at 100 °C and ~1 x 10^{-5} S/cm at 20 °C was achieved.

Table 4.1 Proton conducting polymer electrolytes in the temperature range of 0-100 °C.

Type of electrolyte	Polymer Structure	Doping Ratio[*]	Working Temp. range (°C)	Maximum RT Conductivity (S/cm)	Ref.
PVA-H$_3$PO$_4$			-40 to 40	~ 10^{-5}	(Petty-Week et al., 1988; Polak et al., 1986)
lPEI-H$_3$PO$_4$		0<x<1	25 to 100	~ 10^{-5}	(Tanaka et al., 2000)
PEO-H$_3$PO$_4$		0<x<2	-50 to 100	~ 10^{-5}	(Donoso et al., 1988)
PVA-H$_3$PO$_4$-IPN			-40 to55	10^{-4}-10^{-5}	(Polak et al., 1986)
PEO-PMMA-H$_3$PO$_4$			20 to 60	> 10^{-3}	(Przyluski et al., 1992; Przyluski et al., 1993)
bPEI-H$_3$PO$_4$		0<x<3	25 to 100	10^{-4}	(Daniel et al., 1988; Schoolman et al., 1992; Tanaka et al., 1995)
PAAM-H$_3$PO$_4$		0.6<x<2	-20 to 80	10^{-3}	(Rodriguez et al., 1993)
PAAM-H$_3$PO$_4$-MBA			0 to 100	~ 10^{-3}	(Wieczorec et al., 1995)
Nylon 610-H$_3$PO$_4$		0<x<3	-10 to 70	~ 10^{-3}	(Grondin et al., 1995)

[*] x = number of moles of acid per moles of polymer (repeat unit)

4.2.1.8 PAMA$^+$H$_2$PO$_4^-$ x H$_3$PO$_4$

Poly(diallyldimethylammonium dihydrogenphosphate), PAMA$^+$ H$_2$PO$_4^-$ (M$_w$=200000-350000 g/mol) is a thermally stable quaternary ammonium polymer. Proton conducting blends of composition PAMA$^+$H$_2$PO$_4^-$ x H$_3$PO$_4$, where x denotes the dopant ratio, were prepared by mixing of appropriate amount of polymer with anhydrous acid (Fig. 4.3) (Bozkurt et al., 1999). Blends with 0.5≤x≤2 were totally amorphous as evidenced by WAXS, and could be cast into homogeneous transparent films with thickness as 50-300 μm. TGA results exhibited that PAMA$^+$H$_2$PO$_4^-$ x H$_3$PO$_4$ is stable up to about 200 ^{o}C. DSC data denoted that the addition of H$_3$PO$_4$ to PAMA$^+$H$_2$PO$_4^-$ plasticized the material shifting the T$_g$ from 126 ^{o}C for x=0.5 to –22 ^{o}C for x=2. DC conductivity follows a VTF behavior above T$_g$ at high acid concentrations and Arrhenius behavior at low doping ratios. The conductivity PAMA$^+$H$_2$PO$_4^-$ x H$_3$PO$_4$ increased with increasing x and reached to a maximum value 4x 10^{-4} S/cm at ambient temperature and ~ 10^{-2} S/cm at 100 ^{o}C. The effect of high temperature condensation of acid on the conductivity of PAMA$^+$H$_2$PO$_4^-$ x H$_3$PO$_4$ (with x=1 and x=2) has been investigated by annealing the material at 150-160 ^{o}C and monitoring the conductivities at 20 ^{o}C and 150 ^{o}C.

The analysis of the conductivity with time and temperature indicated that there was almost no change in color and conductivities of the samples. The H$^+$- self diffusion coefficient D$_{PFG}$ (^{1}H) and the phosphor self- diffusion coefficient D$_{PFG}$(^{31}P) of the polymer electrolytes PAMA$^+$H$_2$PO$_4^-$ x H$_3$PO$_4$ (with x=1 and x=2) have been determined with PFG-NMR. Assuming that the D$_{PFG}$ (^{1}H) is the weighted average of the diffusion process D$_{PFG}$(^{31}P) of solvent protons (H$_3$PO$_4$) and a fast diffusion process, D^f$_{PFG}$ (^{1}H), which comprises only acidic protons (H$_3$PO$_4$-H$^+$). The D^f$_{PFG}$ (^{1}H) has been calculated and displayed in graphs as well (Bozkurt et al., 1999). The observation that D$_{PFG}$ (^{1}H) > D$_{PFG}$(^{31}P) signified an inter-phosphate H$^+$- transfer, i.e., structure diffusion, is predominant in both samples. The ratio D$_{PFG}$ (^{1}H)/ D$_{PFG}$(^{31}P) is larger than in pure phosphoric acid, which indicated a stronger immobilization of the H$_2$PO$_4^-$ in the samples than in H$_3$PO$_4$. This immobilization effect became more pronounced at low acid content i.e., PAMA$^+$H$_2$PO$_4^-$ 1 H$_3$PO$_4$ (Figure 4). The voltammograms of PAMA$^+$ H$_2$PO$_4^-$ x H$_3$PO$_4$ (for x = 0 and x = 1) were recorded in a three electrode CV system, using a polymer modified Pt as working electrode (WE) and a Pt counter electrode (CE)

and a reference electrode (Ag/AgCl). It was demonstrated that the electrochemical stability window extends over about 3.0 V. Electrochromic devices based on PAMA$^+$H$_2$PO$_4^-$ 2 H$_3$PO$_4$ have been assembled with a configuration: glass/ITO/WO$_3$/ H$^+$-electrolyte film /H$_x$WO$_3$ /ITO/glass (Bozkurt, 2002).
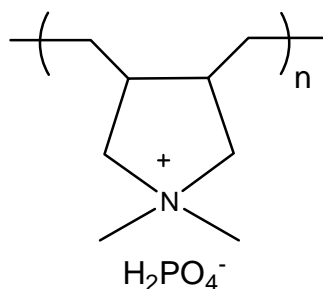
Figure 4.3 Molecular structure of PAMA$^+$H$_2$PO$_4^-$ (Bozkurt et al., 1999).

4.2.1.9 P-4VI x H$_3$PO$_4$

Poly(4(5)-vinyl-imidazole), P-4VI, is insoluble in water and in organic solvents. The P-4VI x H$_3$PO$_4$ blends were prepared by immersion of P-4VI in aqueous solution of phosphoric acid. (Bozkurt and Meyer, 2001b). The doping ratio was varied from 0 to 2. These blends could be cast into homogeneous films. TG results showed that the blends were thermally stable up to about 150 $^\circ$C. The softening temperature of the blends shifted from 77 $^\circ$C for x = 1 to −8 $^\circ$C for x = 2. It was found that ambient temperature conductivity reached to 10^{-4} S/cm for P-4VI 2 H$_3$PO$_4$. Proton conduction mechanism in Poly(4(5)-vinyl-imidazole) were further investigated via dielectric spectroscopy (Pu et al., 2001).

4.2.1.10 PBI x H$_3$PO$_4$

Poly(2,2'-(m-phenylene)-5,5'-bibenzimidazole, PBI (Fig. 4.4) aromatic polymer (pK$_a$=5.5) that has an excellent thermal and chemical stability properties (Samms et al., 1996). Poly(2,5-benzimidazole) (ABPBI) is also another aromatic heterocyclic polymer whose structure is similar to PBI. As polymer electrolytes for high temperature PEM fuel cell, acid doped PBI have been extensively studied (Rikukawa and Sanui, 2000, Schuster and Meyer, 2003, Smitha et al., 2005, Jannasch, 2003, Kerres, 2001). Phosphoric acid doped PBI or ABPBI have been prepared using various approaches like

in-situ casting by incorporation of acid in the polymer solution, post-doping method in bath following casting by solvent drying, etc. Wainright et al. have proposed first PBI/ H_3PO_4 system as a promising electrolyte for medium temperature (150-200 ^{o}C) PEM fuel cells (Wainright et al., 1995). The conductivity of membrane increased with H_3PO_4 content and reached to $2x10^{-2}$ S/cm at 130 ^{o}C and 3.5×10^{-2} S/cm for PBI 5 H_3PO_4 (humidified) at 190 ^{o}C. Wang et al. demonstrated the application of H_3PO_4 doped PBI in H_2/O_2 cell using Pt loaded (0.5 mg/cm^2) carbon electrodes (Wang et al., 1996b). The maximum power density of 0.25W/cm^2 was measured under humidified conditions. The same group used PBI/ H_3PO_4 system (DMAc cast membrane) in direct methanol fuel cells (DMFC) (Wang et al., 1996a). The DMFC fuel cell which was fed 1:2 methanol:water and oxygen provided a maximum power density of 0.1 W/cm^2 at 200 ^{o}C under atmospheric pressure.
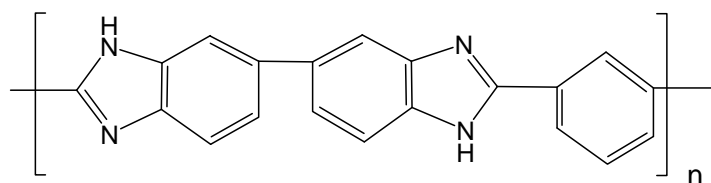
Figure 4.4 Polybenzimidazole, PBI

Samms et al. complexed PBI with sulfuric acid and phosphoric acid and found an improved proton conductivity of 9×10^{-3} S/cm for PBI/H_3PO_4 system (Samms et al., 1996). They reported H_2/O_2 fuel cell results using 0.35 mg Pt/cm^2 on each electrode at atmospheric pressure with anode gas composition: H_2, H_2+25% CO_2 and H_2+25% CO_2+1% CO. Maximum power density was 0.4W/cm^2 at 0.5V.

Bouchet and Siebert worked on anhydrous PBI/H_3PO_4 complexes within a range of the H_3PO_4 doping level from 0.20 to 3.05 (Bouchet and Siebert, 1999). Based on the FT-IR data they concluded that H_3PO_4 protonated the imidazole group of PBI and formed anion i.e., $H_2PO_4^-$ which was linked to the polymer by rather strong hydrogen bonding. The conductivity with x=3.05 was approximately 10^{-5} S/cm at 30 ^{o}C. However, they also reported that anhydrous mixture of PBI with H_2SO_4 exhibited a conductivity of the order of 10^{-4} S/cm at 30 ^{o}C for x=3.25.

Kawahara et al. have measured the conductivity of anhydrous PBI-x H_3PO_4 complexes that exhibited highest proton conductivity of 10^{-4} for x=2.9 at 160 ^{o}C

(Kawahara et al., 2000). Hydrated PBI/strong acid complexes were also prepared by humidifying the films in a 90% RH vessel. Proton conductivity of these complexes (with water uptake 13-26%) increased remarkably at ambient temperature and showed a reverse behavior when the temperature higher than 80 ^{o}C.

Li et al. obtained a conductivity of 4.5 x 10^{-3} S/cm for hydrous PBI 4.5 H_3PO_4 membranes at 25 ^{o}C (Li et al., 2001). The electro-osmotic drag number for water and methanol in PBI/ H_3PO_4 complexes was also reported to be zero compared to Nafion$^{®}$117/H_3PO_4 system with drag numbers 0.2 to 0.6 (Weng et al., 1996). The same group applied PBI 6.5 H_3PO_4 membrane to H_2/O_2 fuel cell at atmospheric pressure and a power density of 0.5 W/cm^2 was obtained at 190 ^{o}C (Li et al, 2000). Furthermore, they worked on PEMFC using PBI 5.3 H_3PO_4 as membrane and searched the CO poison tolerance at higher temperatures (T>125 ^{o}C) and compared with that at low temperatures (Li et al, 2003). They found that near 3% CO in hydrogen could be tolerated at the current density up to 0.8 A/cm^2 at 200 ^{o}C. The CO tolerance was only 0.0025% at 80 ^{o}C at a current densitiy of 0.2 A/cm^2.

Qingfeng et al. further exploited the PBI/ H_3PO_4 complexes and found that the conductivity of these materials insensitive to humidity, but strongly dependent on the acid content, reaching values of 0.13 S/cm at 160 ^{o}C (Qingfeng et al., 2001). Pu et al. proposed that proton transport in PBI/ H_3PO_4 occurs via two different mechanisms (Pu et al., 2002). The first is based on rapid proton exchange among solvent molecules i.e., structure diffusion between phosphate, heterocyclic units of polymer and water. The other is vehicle mechanism that includes the self-diffusion of phosphate moieties and water molecules. They also studied proton conductivity of H_3PO_4 doped poly(*N*-methylbenzimidazole) and poly(*N*-ethylbenzimidazole) with doping level from 2 to 5 (Pu et al., 2004). They found that as the doping level increased from 2 to 5, the conductivity of the membrane increased from 7x10^{-10} to 2x10^{-5} S/cm at room temperature.

He et al. studied the PBI/H_3PO_4 system within a high doping level, from 2.0 to 5.7 (He et al., 2003). They found that as the doping level increased from 2.0 to 5.7, the conductivity of the membrane increased nearly two orders of magnitude from 7.5x10^{-5} to 5.9 x10^{-3} S/cm (95% RH at room temperature). At 80 ^{o}C and 20% RH, an increase in

the conductivity was observed from 5.2 x 10^{-3} S/cm for membranes with doping level of 2.0 to $1.2x10^{-2}$ S/cm for membranes with doping level of 5.7.

4.2.1.11 Chitosan/Methanediphosphonic Acid Composite Material

Other anhydrous proton conducting membrane using a composite of chitosan, one of the basic biopolymers with an amino group, and methanediphosphonic acid (MP), which possesses a large proton exchange capacity was prepared by Honma and Yamada, in 2005 (Fig. 4.5). This chitosan–MP composite material showed the high proton conductivity of 5×10^{-3} S/cm at 150 °C under anhydrous (water-free) conditions. The proton conducting mechanism of the chitosan–MP composite material was due to proton transfer to the proton defect site without the assistance of diffusible vehicle molecules. The utilization of a biopolymer, such as chitosan, for PEMFC technologies is novel and challenging where biological products are usually considered as waste, non-hazardous, and environmentally benign. Especially, the low production cost of the biopolymer is an attractive feature. Anhydrous proton conducting biopolymer composite membranes may have potential not only for PEMFCs operated under anhydrous conditions, but also for bio-electrochemical devices including an implantable battery, bio-sensors. Additionally, the thermal stability of this composite material was found to increase with the mixing ratio of the MP molecule (Yamada and Honma, 2005a).

(a)   (b)
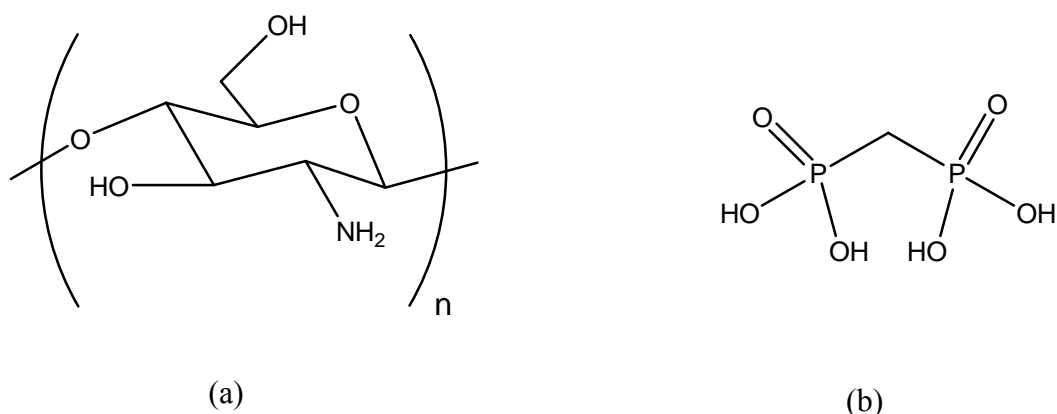
Figure 4.5 Molecular structures of chitosan (a) and methanediphosphonic acid (b) (MP)
(Yamada and Honma, 2005a).

4.2.2 Intrinsic Proton Conductors: Heterocyclic Proton Solvent Tethered Polymers

It has been shown that replacement of water by heterocycles, such as imidazole, pyrazole or benzimidazole leads to proton conductivities at temperatures above 100 $^{\circ}$C (Kreuer et al., 1998). These heterocycles form hydrogen bonded networks and proton transport occurs by hop-turn mechanism via structure diffusion. Although these proton solvents are widely used in closed electrochemical cells, such as supercapacitators and electrochemical devices, the volatility of the heterocycles prevents them from being used in open electrochemical systems, such as fuel cells. Therefore, the use of heterocycles as the proton solvent requires their immobilisation in the polymer membrane in such a way that high mobility of the protonic charge carriers is still provided (Kreuer, 2001).

4.2.2.1 Imidazole Terminated Short Oligo-ethyleneoxide (EO) Chains, imi$_x$

As a first attempt towards a full immobilization of imidazole as proton solvent Schuster et al. prepared imidazole terminated short oligo-ethyleneoxide (EO) chains, imi$_x$ (Table 4.2) (Schuster et al., 2001). They measured the proton conductivity of both pure and triflic acid doped imix. Proton conductivity increased by both increasing x and also the doping ratio. Since the system exhibits VTF behavior it was considered that segmental motions have high effect on proton conductivity. To clarify this statement they analyzed the self-diffusion coefficients D_H of pure imi$_x$ with PFG-NMR and found that D_H increases with x while temperature dependence decreases. T$_g$ values also supported this statement since imi$_5$ has the lowest T$_g$ and imi$_2$ has the highest T$_g$. They obtained a maximum conductivity of 8x10^{-5} S/cm for pure samples and 5x10^{-3} S/cm for triflic acid doped samples at 120 $^{\circ}$C in anhydrous state.

4.2.2.2 Imidazole Functional Polystyrene

Herz et al. prepared fully polymeric solvents with high proton mobility by tethering imidazole terminated side chains with different lengths into polystyrene backbone (Table 4.2) (Herz et al., 2003). The TGA curves of the polymers suggested intrinsic thermal stability up to approximately 200 $^{\circ}$C. Glass transition temperature of

the polymer with short chain was reported as 51 ^oC and that of long chain as 19 ^oC. The conductivities of both polymers showed VFT-type temperature dependence reaching $7x10^{-4}$ S cm^{-1} for short chain polymer and $3x10^{-4}$ S cm^{-1} for long chain one at 200 ^oC. At low temperatures, the conductivity is highest in long chain polymer, while the conductivity at high temperatures is highest in short chain polymer. The authors evaluated this behaviour as reflection of the ambivalent role of hydrogen bonding as already observed for the proton mobility in imidazole compared with pyrazole and discussed for hydrogen bonded systems in general. The immobilised proton donor and acceptor functions exclude any vehicle-type transport and only permit proton mobility via structure diffusion (Grotthuss mechanism) involving proton transfer between the heterocycles with a corresponding reorganisation of the hydrogen bond network as described in more detail

for pure imidazole (Münch et al., 2001).The conductivity of poly(4-vinylimidazole), where the imidazole is directly bonded to the backbone, is comparatively low ($2x10^{-10}$ S cm^{-1} at 150 ^oC) (Bozkurt and Meyer, 2001). Soft spacers, however, seem to allow for an aggregation of the terminating heterocycles and for the formation of dynamical hydrogen bonded structures, supporting high proton mobility (Herz et al., 2003).

4.2.2.3 Imidazole and Benzimidazole Tethered Siloxane

Scharfenberger et al. synthesized imidazole functional cyclic oligomeric siloxane, CImSs and polysiloxane, PImSs (Table 4.2) (Scharfenberger et al., 2006). The materials are reported to be thermally stable up to 200 ^oC. The lowest activation volumes and the highest conductivities are mentioned for the materials with the highest segmental mobilities, i.e. the longest spacers. They obtained highest conductivity of 10^{-3} S/cm for CImSs and $5x10^{-4}$ S/cm for PImSs.

Herz et al. prepared fully polymeric solvents with high proton mobility by tethering benzimidazole units and siloxane network (Table 4.2) (Herz et al., 2003). The highest conductivity of the material is reported as $7x10^{-5}$ S/cm at 150 ^oC.

Persson and Jannasch prepared polydimethylsiloxanes tethered with benzimidazole units via short aliphatic thioether spacers. They reported a highest proton conductivity of $7x10^{-6}$ S/cm at 140 °C (Table 4.2) (Persson and Jannasch, 2005).

Woudenberg et al. immobilized benzimidazole units on several ether acrylate polymer backbone (Table 4.2). Monomers were prepared containing benzimidazole moieties attached by a five carbon tether to the respective functional group, resulting in polymers with Tg values ranging from 88 °C to 113 °C . Increases in Tg over expected values were attributed to decreased mobility induced by aggregation, hydrogen bonding, and π–π interactions of the benzimidazole side chains. The molecular interactions between tethered benzimidazole strongly affects polymer Tg. The acrylate polymer B5A showed conductivity of 0.015 mS/cm at 200 °C, nearly an order of magnitude larger than both B5NB and B5MA (0.0024 mS/cm and 0.0048 mS/cm respectively). The conductivity curves of the electrolytes show VTF behavior. There is a positive effect on conductivity by increasing mobility as seen by comparing B5A and B5MA, however, the competing effect of charge carrier density reduction is clearly seen by comparing B5NB and B5MA. (Woudenberg et al., 2007).

4.2.2.4 Triazole Tethered Systems

While the high proton mobility has been observed in imidazole-based materials, including ionic liquids, oligomers and polymers, the electrochemical stability of imidazole appears to be inadequate for fuel cell applications because of the high electronic density of imidazole ring (Noda et al., 2003, Yang et al., 2001, Deng et al., 2004).

1H-1,2,4-triazole is another promising heterocycle whose molecular structure is similar to imidazole and therefore may conduct protons via structure diffusion mechanism. Compared with imidazole (T_{mp} 89 ^{o}C, T_{bp} 257 ^{o}C), 1H-1,2,4-triazole has a higher melting point (120 ^{o}C) and a similar boiling point (256 ^{o}C) owing to its strong hydrogen bonds. The proton conductivity of pure 1H-1,2,4-triazole is 1.5 x10^{-4} S/cm at 115 ^{o}C and 1.2 x10^{-3} S/cm at melting point 120 ^{o}C. This result proves that self dissociation of 1H-1,2,4-triazole produces highly mobile proton charge carriers (Li et al., 2005).
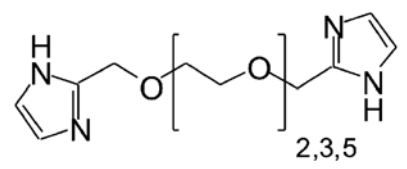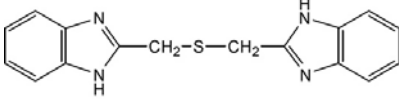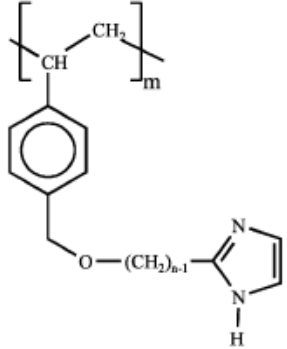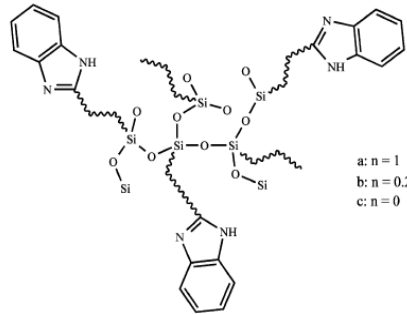
Li et al. intercalated 1*H*-1,2,4-triazole into a sulfonated polysulfone (sPSU). They studied effect of triazole ratio on proton conductivity of the polymer by varying the 1*H*-
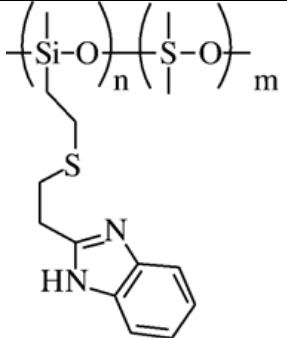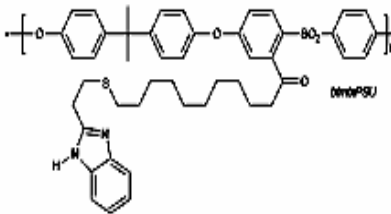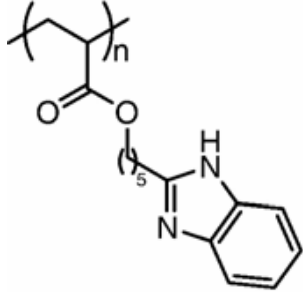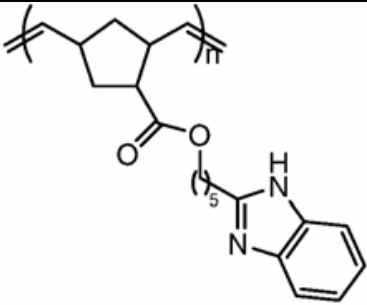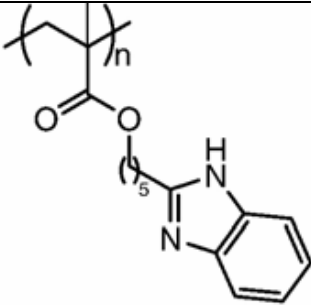
1,2,4-triazole/-SO$_3$H (n) from 4 to 8. The conductivity increased with the concentration of 1H-1,2,4-triazole. For a membrane with n=8, the conductivity reached 5.0x10^{-3} S/cm at 140 °C. Since the sPSU polymer itself has very low ion conductivity under anhydrous (or low humidity) conditions, it is believed that the 1H-1,2,4-triazole is responsible for the observed ionic conductivity of sPSU-1H-1,2,4-triazole membranes. The authors also prepared hybrid inorganic-organic polymers with grafted heterocycles such as imidazole and triazole (Table 4.2). 1H-1,2,4-triazole grafted onto the hybrid inorganic-organic polymer network enhanced the proton conductivity of the membranes doped with H$_3$PO$_4$. This may be attributed to the low-barrier hydrogen bonds formed between 1,2,4-triazole and H$_3$PO$_4$ molecules because the pKa values of protonated 1,2,4-triazole and H$_3$PO$_4$ are about the same (Garcia-Viloca et al., 1997). Proton conductivity of the membrane with grafted 1H-1,2,4-triazole is higher than that without grafted heterocycles, but the grafted-imidazole (Im) reduced the proton conductivity under similar conditions. The maximum proton conductivity of 1H-1,2,4-triazole grafted polymer is about 5x10^{-3} S/cm at 140 $^{\circ}$C and it is about 10^{-6} S/cm for imidazole grafted polymer. (Li et al., 2005).
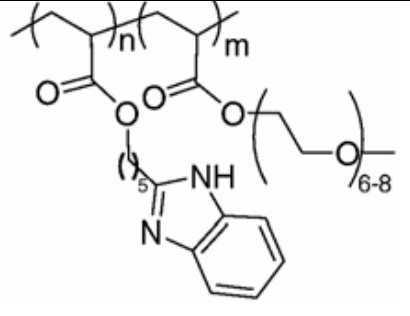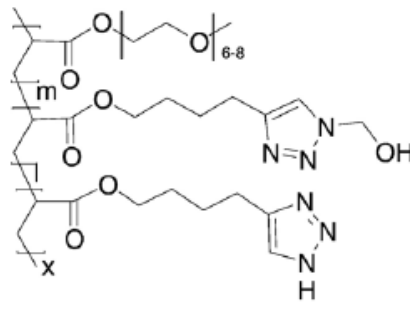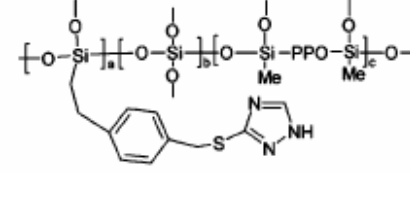
Martwiset et al. immobilized 1,2,3-triazole and N-methyl hydroxy triazole units on acrylate monomers and prepared copolymers with poly(ethylene glycol) methyl ether acrylate. The composition of the triazole containing polymers was varied in order to study the effects of charge carrier density, polymer matrix mobility and heterocycle nature on the proton conductivity of the resulting materials. The proton conductivity decreased as the ratio of N-methyl hydroxy triazole units increased. The authors compared the conductivity of T5A-4-30PEG with that of B5A-35PEG, an analogous benzimidazole polyacrylate previously reported by Woudenberg et al. (Woudenberg et al., 2007). The conductivity of T5A-4-30PEG is approximately 0.5 to 1.5 orders of magnitude higher than B5A-35PEG at 200 °C and 80 °C respectively. The improved conductivity may be attributed to several factors, the lower Tg of
T5A-4-30PEG (− 24 °C vs. 2 °C for B5A-35PEG), the decreased basicity of the protonic charge carrier (pKa of 1,2,3-triazole = 9.26, pKa of benzimidazole = 12.17), (Zhou et al., 2005; Sari and Covington, 2005) and a lower number of conformational changes necessary for proton hopping in 1,2,3-triazole vs benzimidazole (Zhou et al., 2006). The conductivity increases as a function of absolute and a normalized temperature as PEGMEA incorporation increases until reaching a limit at 30 mol %.

This finding indicates that Tg reduction with PEG in 1,2,3-triazole systems can counteract the associated reduction in charge carrier density. The lower conductivity observed for terpolymers with higher PEGMEA fractions suggests that at those compositions the decrease in charge carrier concentration becomes the limiting factor for proton transport over the backbone mobility. Doping the polymers with TFA resulted in further conductivity increases ranging from 0.5 to 1.5 orders of magnitude compared to the undoped membranes (Martwiset et al., 2007).

Table 4.2 Structures, glass transition temperatures and maximum proton conductivities of some heterocyclic proton solvent tethered polymers.

Polymer	Structure	T_g ^oC	Proton Conductivity S/cm	Ref.
Imi_x		-7.9 -13.9 -24.4	5×10^{-3} at 120 ^oC	(Schuster et al., 2001)
bBImTP		-	3×10^{-5} at 140 $\circ C$	(Günday et al., 2007)
Imidazole Terminated Polystyrene		51 n=6 19 n=12	7×10^{-4} at 200 ^oC	(Herz et al., 2003)
IPTS		-	7×10^{-5} at 150 ^oC	(Herz et al., 2003)

Polysiloxane copolymer with tethered benzimidazole (~32 mol%)		~50	7×10^{-6} at 140 °C	(Persson and Jannasch, 2005)
PSU tethered with benzimidazole (bimi1.7PSU)		83	$\sim 4 \times 10^{-8}$ at 180 °C	(Persson et al., 2006)
B5MA		113	4.8×10^{-3} at 200 °C	(Woudenberg et al., 2007)
B5NB		98	2.4×10^{-3} at 200 °C	(Woudenberg et al., 2007)
B5A		88	1.5×10^{-2} at 200 °C	(Woudenberg et al., 2007)

B5A-PEGMEA 35		2	1.1×10^{-2} at 200 °C	(Woudenberg et al., 2007)
T5A-4-30PEG		~ 25	1.8×10^{-5} at 200 °C	(Martwiset et al., 2007)
2MDSPPO-2TEOS-2Si4Tri-5H3PO4			5×10^{-3} at 140 °C	(Li et al., 2005)

4.2.3 Polymer/Heterocycle Hybrid Electrolytes

4.2.3.1 PVPA-Heterocycle Composite Materials

Yamada and Honma have prepared the acid–base composite materials by mixing of a strong phosphonic acid polymer poly(vinylphosphonicacid) (PVPA) with the high proton exchange capacity and an organic base heterocycle, such as imidazole (Im), pyrazole (Py), and 1-methylimidazole (MeIm) (Fig. 4.6) (Yamada and Honma, 2005b). This PVPA-heterocycle composite material exhibited a large proton conductivity of 7×10^{-3} S/cm at 150 °C under anhydrous condition. Additionally, the thermal stability of composite material was found to increase with the mixing ratio of the heterocycle.
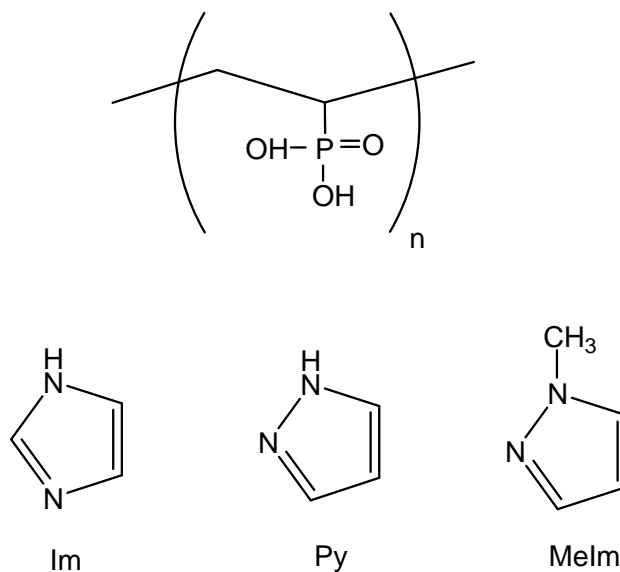
Figure 4.6 Molecular structures of poly(vinylphosphonicacid) (PVPA) , imidazole (Im),
pyrazole (Py), and 1-methylimidazole (MeIm) (Yamada and Honma, 2005b).

Anhydrous proton conductivity of PVPA-heterocycle composite materials showed differences of approximately one order of magnitude, depending on the molecular structure of basic heterocycles. These different conductivities of composite materials are due to the pKa value of heterocyclic molecules. The pKa values of heterocycle molecules (Acheson, 1976) and the maximum proton conductivity at 150 °C under anhydrous condition are listed in Table 2.1. The basicity of heterocycle molecules of Im is larger than that of Py (see the pKa1 value in Table 4.3). Clearly, the conductivity of PVPA-Im composite material is larger than PVPA-Py composite material. These results suggest that pyrazole molecule with the low basicity do not act as a proton donor and acceptor in composite material since the free proton from the PVPA molecule could not strongly interacts with non-protonated –N= group of pyrazole ring. In contrast, the pKa1 value of MeIm molecules is as same as that of Im molecules. However, the conductivity of PVPV-MeIm composite material is lower than that of PVPA-Im. This phenomenon is due to the molecular structure of imidazole. The Im molecules have been reported the construction of molecular cluster, consisting of approximately 20 molecules (Acheson, 1976), through the intermolecular hydrogen bonding.

As a result, PVPA-Im composite material might possess fast proton transfer of inter-heterocycle molecules in the composite material. However, MeIm molecules do

not construct the molecular cluster with the intermolecular interaction in membrane and cannot provide fast proton transfer kinetics in inter heterocycle molecules. Based on the basicity and clustering mechanism, PVPA-Im composite material are supposed to possess the highest proton conductivity of 7×10^{-3} S/cm at 150 °C under anhydrous condition in many different types of PVPA-heterocycle composite materials. These results suggest that the basicity and molecular structure of heterocycle in acid-base composite material are important factors to obtain the anhydrous proton conductivity at the intermediate temperature condition (Yamada and Honma, 2005b).

Table 4.3 Maximum proton conductivities of PVPA-heterocycle composite material and acid dissociation constant (pKa values of various heterocycle molecules) (Acheson, 1976).

PVPA-heterocycle	Maximum conductivity at 150 °C (S/cm)	Pka value of heterocycle	
		Pka1	Pka2
PVPA-Im	7×10^{-3}	7.2	14.5
PVPA-Py	8×10^{-4}	2.5	14
PVPA-MeIm	1×10^{-3}	7.4	

4.2.3.2 PAA/Imidazole Composite Membranes

In 2003, anhydrous proton conducting polymer electrolytes have been prepared by entrapping imidazol (Im) in polyacrylic acid (PAA) with various stoichiometric ratios, x, to form PAAxIm (x is the number of moles of Im per polymer repeat unit) (Fig. 4.7) (Bozkurt et al., 2003). Polymer electrolytes, PAAxIm (with x = 0.5 and 1) can be cast into transparent, homogeneous films which are thermally stable up to 200 °C. From FT-IR spectra it is evident that hydrogen bonds exist between protonated and unprotonated Im units. With increasing Im content the glass transition temperature decreases while their conductivity increase, reaching 10^{-3} S/cm at 120 °C.
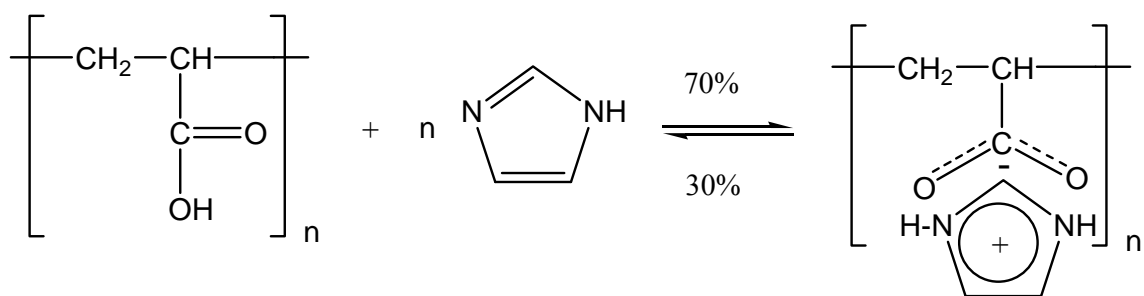
Figure 4.7 Illustration of the protonation of imidazol upon blending with PAA (Bozkurt et al., 2003).

It was previously mentioned that the membrane materials based on carboxylic acid groups shows no significant proton conductivity even at higher level of hydration. Because –COOH groups are less sensitive to hydrolysis and higher pKa values (Kreuer, 1996).

The intercalation of imidazol with different doping ratio, x into PAA as Brønstedt acid increased the conductivity PAAxIm membranes. The reason may be imidazol, like water, acts as proton donor and acceptor in the proton conduction process. In this sense it behaves amphoteric but with respect to other compounds they are more basic than water (Kreuer, 1998). FT-IR of PAAxIm confirmed that imidazol is partially protonated from "free" nitrogen side. A Grotthuss type diffusion mechanism may explain the proton diffusion process within protonated and unprotonated heterocycles. Because the protonic defect may cause local disorder by forming (. . . Him-(HimH+)-imH. . .) configuration as discussed in the literature (Münch et al., 2001). The use of imidazol in a suitable acidic host polymer to increase the concentration of defect protons may also technological interest. Further systems like PAMPSA-imidazole are under investigation and will be communicated soon.

4.2.3.3 Benzimidazole/Monododecyl Phosphate Molecular Hybrids

It had been reported that a glass-filter supported monododecyl phosphate/benzimidazole mixed material shows a high proton conductivity of $1x10^{-3}$ S/cm at T = 150 ^{o}C underwater-free conditions along with a high thermal stability (Yamada and Honma, 2003). Even other acid–base hybrid materials resulted in the

same anhydrous conductor at elevated temperatures (Yamada and Honma, 2004a, Yamada and Honma, 2004b). Kim and Honma investigated the effects of monododecyl phosphate (MDP) doping to benzimidazole (BnIm) by IR, TG, XRD, proton conductivities. The XRD results showed new phases different from the crystal structures of MDP and BnIm (Fig. 4.8), and the doping of MDP displayed the peaks of BnIm due to the extinction rule of reflection. The hybrids showed a high proton conductivity of 1×10^{-2} S/cm above 100 °C under a non-humidified (anhydrous) condition (Kim and Honma, 2005).

(a)   (b)
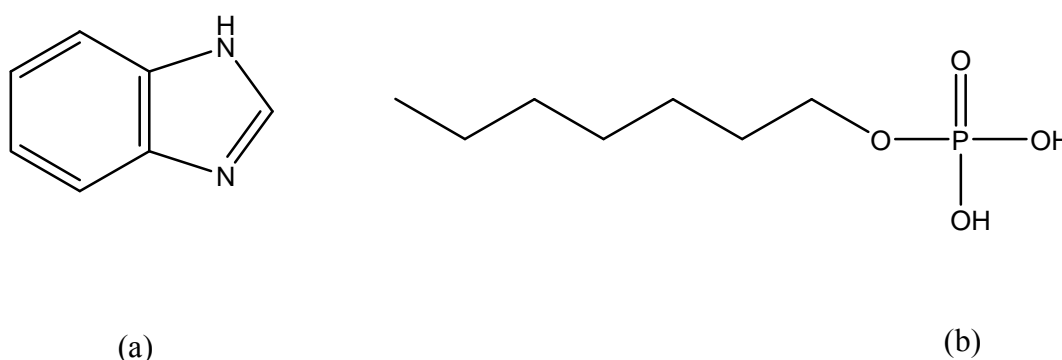
Figure 4.8 Molecular structures of (a) benzimidazole and (b) monododecyl phosphate
(Yamada and Honma, 2003).

4.2.3.4 Alginic Acid/Imidazole Composite Material

Other anhydrous proton conductor consisting of alginic acid (AL), one of the acidic biopolymers, and imidazole (Im) molecules, one of the basic heterocyclic molecules was reported by Yamada et al. in 2004. This AL-Im ($r \geq 20$) composite material indicated the high proton conductivity of 2×10^{-3} S/cm at 130 °C. On the other hand, the activation energy, such as 1.2-1.6 eV, at $r \leq 1$ is extremely larger than that of other reported materials. This high activation energy is due to the long distance between the hopping sites. Additionally, the proton hopping distance of pure AL or small mixed material ($r \leq 0.5$) was too long to hop to neighboring site, as a result, these materials could not show any measurable proton conductivity ($< 10^{-8}$ S/cm) (Yamada and Honma, 2004b).

The bimolecular composite material, such as chitin phosphate-hetrocyclic molecules composite materials as an anhydrous proton conducting membrane was reported by (Yamada and Honma 2004a). In these cases, the composite materials showed the high proton conductivity of $\geq 10^{-3}$ S/cm at 150 °C under anhydrous condition. Additionally, these materials had a high thermal stability. However, AL-Im composite materials did not indicate the satisfactory conductivity and thermal stability in comparison with the reported materials (Yamada et al., 2003, Yamada et al., 2004b). One of the reasons might be the effect of pKa value (pKa = 3.1) of –COOH group in AL (Jang et al., 1999). Phosphonic acid is stronger than carboxylic acid. The phosphonic acid group and basic group forms a strong acid-base complex in the composite membrane, as a result the free proton from phosphonic acid strongly interacts with non-protonated –n= (Yamada et al., 2003, Yamada et al., 2004a). However a weak acid, such as –COOH group in AL, cannot form the strong acid-base in composite membrane and not provide enough mobile-protons to Im molecules, so that AL-Im composite showed the lower anhydrous proton conductivity than the phosphonic acid composite materials (Yamada and Honma, 2004b).

4.2.3.5 Adipic Acid/Benzimidazole Hybrid Electrolytes

Karadedeli et al. investigated several blends of a diacid, adipic acid (AA) (Fig. 4.9) and heterocyclic base, benzimidazole (BnIm). Adipic acid has very low proton conductivity ($\sim 10^{-11}$ S/cm) in crystalline form. The conductivity of the blends increased with BnIm and reached a maximum conductivity of 4×10^{-3} S/cm at 130 °C (Karadedeli et al., 2005).

$$
\underset{\text{HOC (CH}_2)_4\text{ COH}}{\overset{\displaystyle \overset{O}{\|} \qquad\quad \overset{O}{\|}}{}}
$$
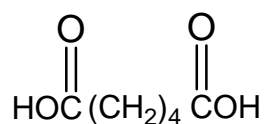
AA

Figure 4.9 Moleculer structure of AA (Karadedeli et al., 2005).

From DSC results, it can be concluded that such conductivity increase within this temperature regime may be the effect of first-order transition (melting) onto the ionic

conductivity of the samples. At higher temperatures, (T > 373 K) the conductivities of these samples are very close to each other irrespective of their BnIm content. High BnIm doping levels (BnIm$_2$AA) result in higher conductivity even at lower temperatures. This behavior may reflect the ambivalent role of hydrogen bonding as already observed for the proton mobility in heterocyclic systems (Kreuer et al., 1998). Previously the proton conductivity in anhydrous heterocycles, i.e. imidazole and pyrazole, and their mixtures with H$_2$SO$_4$ and H$_3$PO$_4$ were investigated (Kreuer et al., 1998, Schuster and Meyer, 2003).

The protonic defects are created by protonation of heterocycles which act as solvent for protons and it is the dynamics of these solvent molecules which lead to the mobility of the protonic defects, i.e. intermolecular proton transfer and structural reorganization by hydrogen bond breaking and forming processes (structure diffusion). The IR spectra of the BnImxAA indicate the partial protonation of benzimidazole which occurs from the free N side forming benzimidazolium ion. Therefore, at higher temperatures, protons can be rapidly transferred to neighbor molecule with small activation energy. Similar behavior was observed in PAA-imidazole and mono-dodecylphosphate (MDP)-benzimidazole mixed materials (Bozkurt et al., 2003, Yamada et al., 2003). The BnImxAA blends showed a maximum conductivity of 4x10^{-3} S/cm at 130 °C in anhydrous state. The materials which comprise –CO$_2$H acidic functional groups as part of their constitutional unit have not been preferred as proton conductors since these units are less sensitive to hydrolysis, have higher pKA values and hence yield low conductivity. This work was demonstrated that anhydrous, high proton conductive organic electrolytes can also be obtained when –CO$_2$H containing materials are doped with benzimidazole (Karadedeli et al., 2005).

4.2.3.6 Nafion/Triazole and Nafion/Benzimidazole Composite Membranes

Kim et al. used 1,2,4-Triazole and benzimidazole as proton solvent in Nafion system. Since 1,2,4-Triazole and benzimidazole have low volatility (bp = 260 °C and >360 °C, respectively) they can be used for applications over 100 °C. The thermal stabilities of the Nafion–l,2,4-triazole- and Nafion–Bz-blend membranes decreased with an increase in the amount of 1,2,4-triazole and Bz. the conductivity increased with the

concentration of 1,2,4-triazole and Bz. The conductivity of the membranes with n = 14.5 (n is defined as the ratio of 1,2,4-triazole to –SO₃H in Nafion–1,2,4-triazole) and with n = 8.5 (n is defined as the ratio of Bz to–SO₃H in Nafion–Bz) reached 2.3×10^{-2} S/cm at 160 °C and 8.64×10^{-3} S/cm at 200 °C, respectively. Because dry Nafion itself has a very low proton conductivity above 100 °C it is speculated that the observed ionic conductivity arises from the diffusion of protonated 1,2,4-triazole or Bz and intermolecular proton transfer (Kim et al., 2007).

4.2.3.7 PAMPS/Triazole and PVPA/Triazole Composite Membranes

Günday et al. have prepared novel proton conducting polymer electrolytes through blending of 1,2,4-triazole with acidic host polymer, poly(2-acrylamido-2-methyl-1-propanesulfonic acid) (PAMPS) and Poly(vinylphosphonic acid) (PVPA) (Fig. 4.10) (Günday et al., 2006). Using FTIR spectra they confirmed the protonation of the heterocyclic ring and proton conductivity of the electrolytes increased with Tri content. They attributed this to the increase in the unprotonated nitrogen sites as in the case of imidazole. They reported a maximum anhydrous proton conductivity of 9.3×10^{-4} S/cm for $PAMPSTri_2$ at 140 °C and 2.3×10^{-3} S/cm for $PVPATri_{1.5}$ at 120 °C.
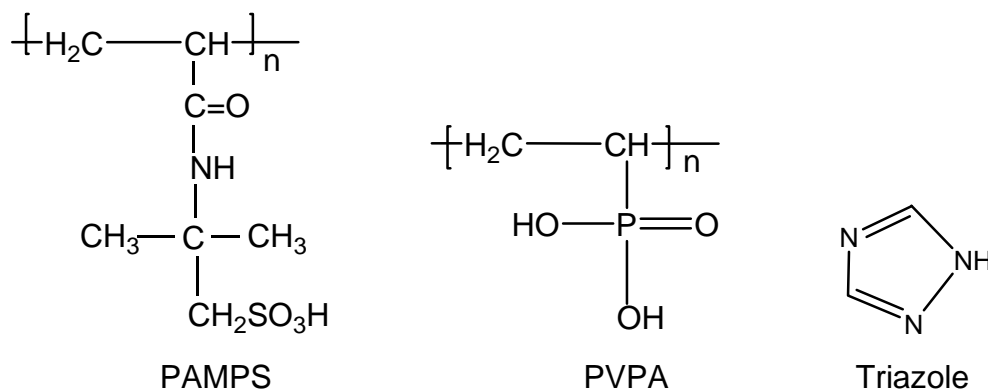
Figure 4.10 Molecular structures of PAMPS, PVPA and Triazole (Günday et al., 2006).

4.2.3.8 PSSA/Triazole and PSSA/imi3 Composite Membranes

Göktepe et al. produced PSSA by sulfonation of polystyrene and then doped PSSA with Tri and imi3 at several compositions, to obtain PSSATri*x* and PSSAimi3*x* electrolytes. (Fig. 4.11) (Göktepe et al., 2008). The materials are reported to be thermally stable up to 200 ∘C and from DSC results they observed the plasticization effect of the dopants. The intrinsic proton conductivity of pure imi3 was reported to be about 5×10^{-5} Scm^{-1} at 120 ∘C (Kreuer et al., 1998). The insertion of imi3 into PSSA increased the proton conductivity of the PSSAimi3$_{0.5}$ to 5×10^{-4} Scm^{-1} at ambient temperature. It is reasonable that the proton transport in PSSAimi30.5 occurs between terminating imidazole units through intermolecular proton transport (structure diffusion). These proton solvents aggregate in such a way that long-range proton transport can be enhanced by forming local disorder through the hydrogen bonding network, i.e. Him–(HimH+) – imH (Kreuer et al., 1998). Also, proton conductivity of anhydrous materials based on benzimidazole, BnIm-doped PSSA, was reported (Bozkurt, 2005). PSSABnIm*x* blends showed a maximum conductivity of 5×10^{-4} Scm^{-1} at 150 ∘C in the anhydrous state. The proton conductivity of anhydrous PSSATri$_{1.5}$ electrolyte is at least five orders of magnitude higher than that of PSSABnIm1.5 at room temperature. PSSATri$_1$ showed a highest conductivity of 0.016 S cm^{-1} at 150 ∘C.
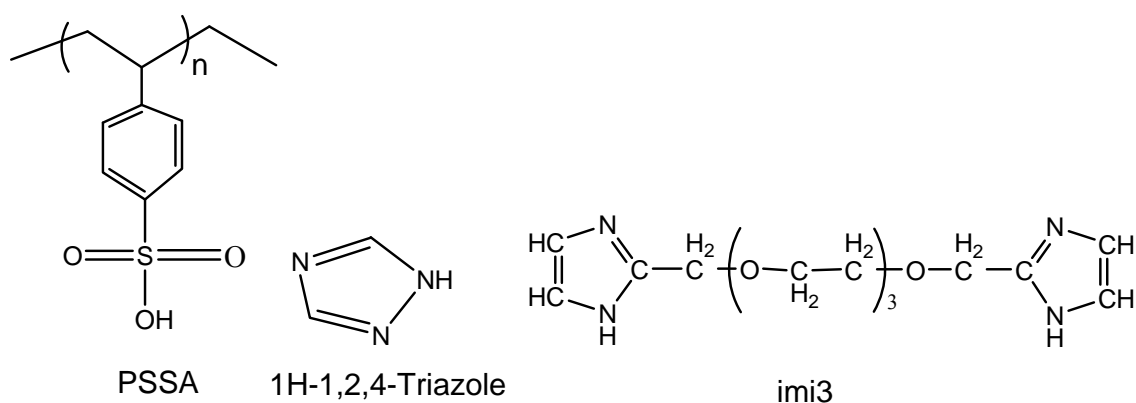
Figure 4.11 Molecular structures of PSSA, Triazole and imi3 (Göktepe et al., 2008).

CHAPTER 5

EXPERIMENTAL

5.1 Materials and Preparation

Glycidyl methacrylate (>97%) (Fig. 5.1), 1H-1,2,4-triazole (>98%) (Fig. 5.1), 3-amino-1,2,4-triazole (>95%) (Fig. 5.1) and 5-aminotetrazole monohydrate (>97%) (Fig. 5.2) were supplied from Aldrich Chemical Company. Ortho-Phosphoric acid (>99%), Toluene (>99%) and Diethlyether (>99.5%) were purchased from Merck. Trifluoromethanesulfonic acid (>99%) and DMF (>99) were obtained from Fluka and they are all reagent grade and were used as received.

5.1.1 Synthesis of Poly (glycidyl methacrylate), PGMA

Poly (glycidyl methacrylate) (Fig. 5.1) was produced by free radical polymerization of glycidyl methacrylate (5.0 g) in toluene (100 ml) using AIBN (1% mol) as initiator. The reaction mixture was purged with nitrogen and the polymerization reaction was performed at 75 ^{0}C for 4 h. Transparent solution of the polymer was precipitated in diethyl ether and the product was dried at 50 ^{0}C under vacuum.

5.1.2 Synthesis of PGMA-Triazole, PGMATri and PGMA-Aminotriazole, PGMAATri

1H-1,2,4-triazole (Mw=69.1 g/mol) (Tri) and 3-amino-1,2,4-triazole (Mw=84.08 g/mol) (ATri) were attached to PGMA according to following procedure described by Moore et al (Moore et al., 1992). After 4 h polymerization of GMA in toluene, azole groups were added into the solution with stoichometric ratio 1:5 (GMA: Azole). The temperature was set to 100 ^{0}C and the mixture was stirred for 20 h (Fig. 5.1). The resulting solid mixture was filtered and dialized against water to remove excess azoles.

After dialysis, it was filtered and dried at 50 ^{0}C under vacuum. Light yellow and rigid polymers were obtained. Polymers are insoluble in common organic solvents and in aqeous medium.
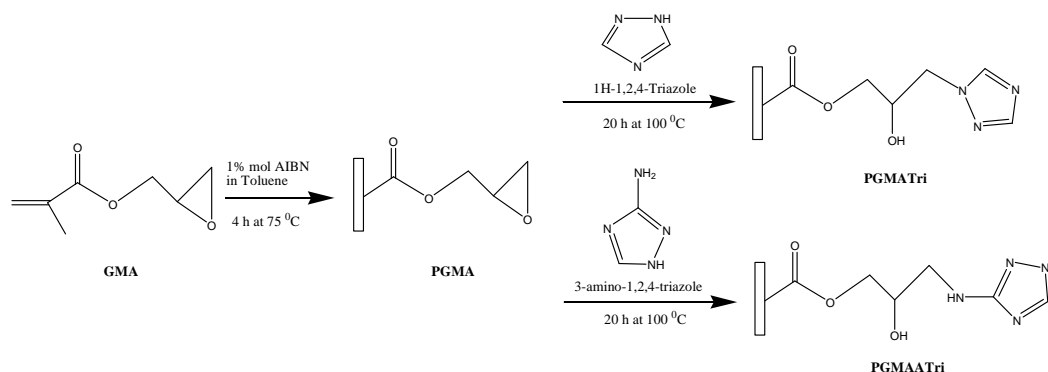
Figure 5.1 Synthesis of PGMA, PGMATri and PGMAATri

Doping was performed by dispersing the polymer in solvent, then adding acid with different ratios, x (i.e. x is the number of moles of acid per moles of triazole unit in the polymer). After evaporating the solvent, polymers were dried completely in a vacuum oven. Soft powder materials were obtained. The doping procedure is summarized in Tables 5.1 and 5.2.

Table 5.1 Preparation of acid doped PGMATri

Doping acid	x	PGMATri (85 % Tri)	Acid mole	Solvent
Triflic acid	0.2	0.7 g (2.82 mmol Tri)	0.0846 g (0.564 mmol)	15 ml methanol
Triflic acid	0.4	0.7 g (2.82 mmol Tri)	0.1692 g (1.128 mmol)	15 ml methanol
H_3PO_4	1	0.5 g (2.00 mmol Tri)	0.197 g (2.00 mmol)	5 ml water
H_3PO_4	3	0.5 g (2.00 mmol Tri)	0.591 g (6.00 mmol)	5 ml water
H_3PO_4	4	0.5 g (2.00 mmol Tri)	0.788 g (8.00 mmol)	5 ml water

Table 5.2 Preparation of acid doped PGMAATri

Doping acid	x	PGMAATri (84 % ATri)	Acid mole	Solvent
Triflic acid	0.2	0.71 g (2.67 mmol ATri)	0.0801 g (0.534 mmol)	15 ml methanol
Triflic acid	0.4	0.71 g (2.67 mmol ATri)	0.1602 g (1.068 mmol)	15 ml methanol
H_3PO_4	1	0.5 g (2.00 mmol ATri)	0.180 g (1.88 mmol)	5 ml water
H_3PO_4	2	0.5 g (2.00 mmol ATri)	0.360g (3.76 mmol)	5 ml water

5.1.3 Synthesis of PGMA-aminotetrazole, PGMAATet

5-aminotetrazole was attached to PGMA according to following procedure described by Moore et al (Moore et al., 1992). After 4 h polymerization of GMA in toluene, 5-aminotetrazole was added into the solution with stoichometric ratio 1:5 (GMA: ATet). The temperature was set to 100 ^{0}C and the mixture was stirred for 20 h. The resulting solid mixture was filtered and washed with DMF to remove unreacted aminotetrazole. The polymer was dialyzed against water for 2 days. After dialysis it was filtered and dried at 50 ^{0}C under vacuum. White powder polymer was obtained.
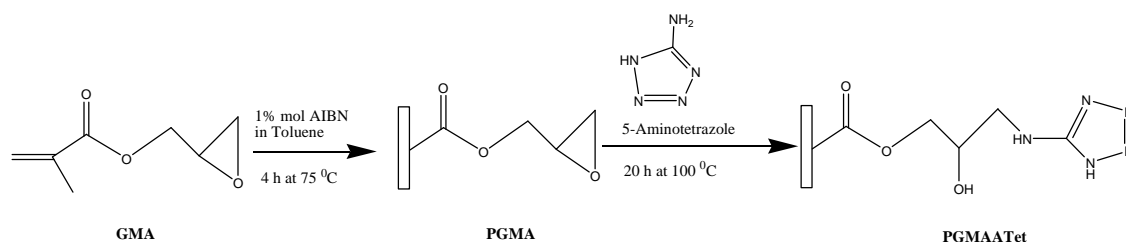
Figure 5.2 Synthesis of PGMAATet

Doping was performed by dispersing 0.5 g of the polymer in water, then adding H_3PO_4 with different ratios (x). X is the number of moles of acid per moles of aminotetrazole unit in the polymer. After evaporating the water, soft polymers were dried completely in a vacuum oven. The doping procedure is summarized in Table 5.3.

Table 5.3 Preparation of acid doped PGMAATet

Doping acid	x	PGMAATet (78 % ATet)	Acid mole	Solvent
H_3PO_4	1	0.5 g (1.72 mmol ATet)	0.168 g (1.72 mmol)	5 ml water
H_3PO_4	2	0.5 g (1.72 mmol ATet)	0.336 g (3.44 mmol)	5 ml water
H_3PO_4	4	0.5 g (1.72 mmol ATet)	0.672 g (6.88 mmol)	5 ml water

5.2 Characterizations

5.2.1 FT-IR Spectroscopy

Fourier-Transform IR (FTIR) is most useful for identifying chemicals that are either organic or inorganic. It can be utilized to quantitate some components of an unknown mixture. It can be applied to the analysis of solids, liquids, and gasses. The term Fourier Transform Infrared Spectroscopy (FTIR) refers to a fairly recent development in the manner in which the data is collected and converted from an interference pattern to a spectrum. FTIR can be used to identify chemicals from spills, paints, polymers, coatings, drugs, and contaminants. FTIR is perhaps the most powerful tool for identifying types of chemical bonds (functional groups). The wavelength of light absorbed is characteristic of the chemical bond as can be seen in this annotated spectrum. FT-IR spectra of pure and acid doped azole functional PGMA were scanned using a Mattson Genesis II spectrophotometer as KBr pellets between 400-4000 cm^{-1}. The spectra were analyzed to verify both azole functionalization of PGMA and dopant interaction with azole units.

5.2.2 Solid State ^{13}C CP-MAS NMR Measurements

Solid state ^{13}C CP-MAS NMR studies of the samples were performed using a Bruker Avance spectrometer at a Larmor frequency of 176.06 MHz in the Max-Planck Institute for Polymer Research, Mainz, Germany. All spectra were recorded with 1ms

CP contact time, 15 kHz MAS frequency and 2 s relaxation delay time. ^{13}C CP-MAS NMR spectra of the samples were recorded at ~305 K.

### 5.2.3 Thermogravimetry (TG) Analysis

Thermogravimetry analysis (TGA) is based on the measurement of the weight loss of the material as a function of temperature, or isothermally as a function of time, in an atmosphere of nitrogen, helium, air, other gas, or in vacuum. TGA curve provides information concerning the thermal stability of the initial sample, intermediate compounds that may be formed and of the residue if any. In addition to thermal stability, the weight losses observed in TGA can be quantified to predict the pathway of degradation or to obtain compositional information. The ability to vary atmosphere during the TGA evaluation, particularly from an inert to a reactive gas, provides additional information about a material composition and its stability. The experimental data offer more sophisticated understanding of reactions occurring at materials heating. Thermal stabilities of the pure and acid doped azole functional PGMA were examined by with a Perkin Elmer Pyris 1 TG analyzer. The samples (~ 10 mg) were heated from room temperature to 800 ^{o}C under N_2 atmosphere at a scanning rate of 10 ^{o}C/min. The effect of dopant on thermal stability was determined using TG curves.

5.2.4 Differential Scanning Calorimetry (DSC) Analysis

DSC measures the temperatures and heat flow associated with transitions in materials as a function of time and temperature. It determines transition temperatures, melting and crystallization, and heat capacity. In heat flux insruments, the sample and reference are heated from the same source and the temperature difference is measured. In amorphous polymers DSC shows the glass transition temperature (T_g) and presence of single T_g verifies the homogeneity of the polymer. DSC measurements of pure and acid doped azole functional PGMA were carried out on a Netzsch Differential Scanning Calorimeter DSC 404 C Pegasus under nitrogen atmosphere and heating-cooling curves were recorded at a rate of 10 ^{o}C/min. The glass transition temperatures were determined from the second heating curves and the effect of dopant on glass transition temperature was studied.

5.2.5 Proton Conductivity Measurements

The proton conductivity studies of the samples were performed using a SI 1260-Schlumberger impedance spectrometer in the Max-Planck Institute for Polymer Research, Mainz, Germany. The conductivities were measured in the frequency range 1 Hz to 1 MHz at 10 ^{o}C intervals. The temperature was controlled with a Novocontrol cryosystem, which is applicable between -150 and 400 ^{o}C with a precision of 0.01 ^{o}C. The hot pressed pellets of the samples with a diameter of 10 mm and thickness of about 0.2-0.3 mm were sandwiched between two gold-coated electrodes (Fig. 5.3) and their conductivities were measured with 10 ^{o}C intervals under dry-nitrogen atmosphere.
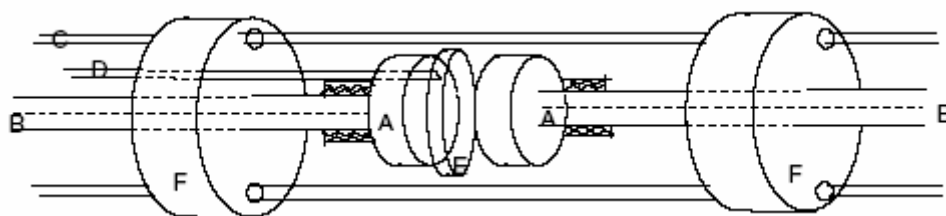
Figure 5.3 Schematic drawing of conductivity cell. (A) Gold plated electrodes, (B) platinum wire, (C) adjustable Hylam screws, (D) thermocouple, (E) membrane, (F) PTFE disks (Smitha et al., 2005).

CHAPTER 6

RESULTS AND DISCUSSION

6.1 FT-IR Studies

6.1.1 FT-IR of PGMA, PGMATri and PGMAATri

FT-IR spectra of PGMA, triflic and phosphoric acid doped PGMATri are represented in Fig. 6.1. In PGMA the carbonyl group gives a strong peak at 1720 cm^{-1} and the strong peaks at 1140 cm^{-1} and 1260 cm^{-1} are attributed to C-O stretching of the ester group (Hirose et al., 2002). The absorption at 900 cm^{-1} is assigned to stretching vibration of the epoxy group which disappeared up on triazole functionalization (Nanjundan et al., 2005). PGMATri exhibited a medium absorption at 1577 cm^{-1} and 1450 cm^{-1} due to C=N and C-N stretching of the triazole ring (Krishnakumar and Xavier, 2004). After doping PGMATri with triflic acid the intensity of the peak at 1577 cm^{-1} decreases and the intensity of the peaks at 1510 cm^{-1} and 1450 cm^{-1} increase which may show the protonation of the triazole ring. Additionally, the peak which appears at 3100 cm^{-1} shows the N-H absorption. Doping of PGMATri with H_3PO_4, two strong peaks appear near 500 cm^{-1} and 1000 cm^{-1} which are attributed to PO_2 bending vibration of ($H_2PO_4^{2-}$) and P-O symmetric stretching of H_3PO_4 (Bouchet and Siebert, 1999). The carbonyl stretching band at 1725 cm^{-1} decreases and broadens due to protonation of C=O bond. In addition, the disappearance of the triazole ring stretching at 1550 cm^{-1} (C=N) as well as the formation of a broad band at 1940-1960 cm^{-1} may indicate proton exchange reactions (Günday et al., 2006). Similar absorption bands are also present in FT-IR spectra of PGMAATri (Fig. 6.2) except a new absorption at 1640 cm^{-1} coming from amine bending vibration.
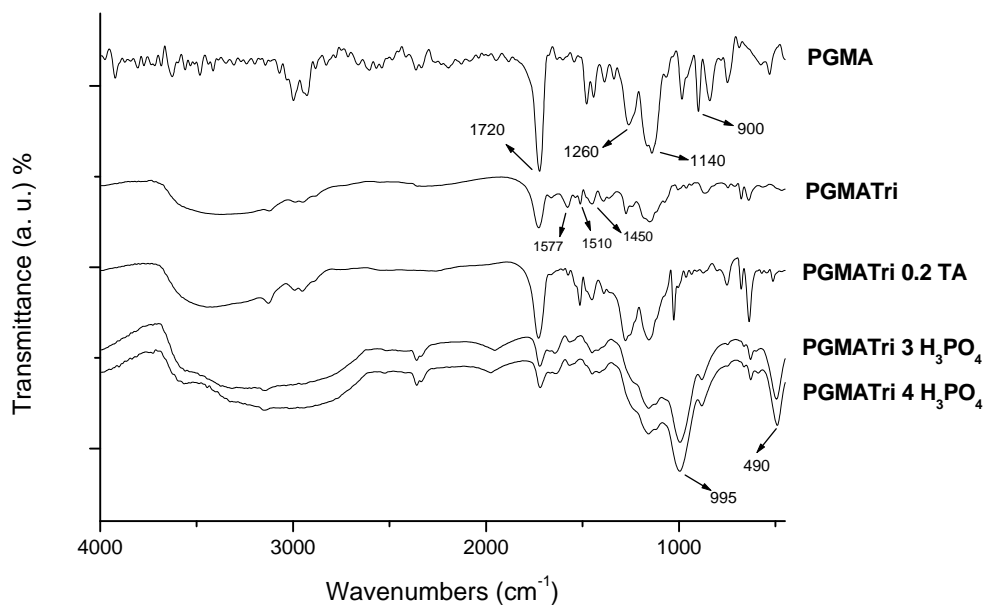
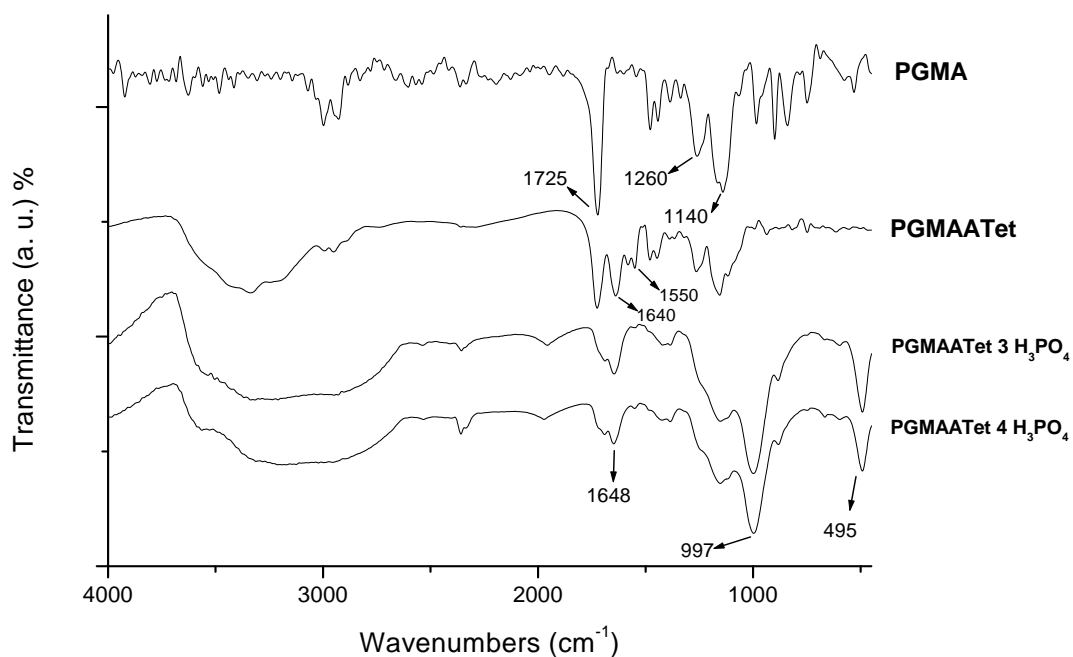**Figure 6.1** FT-IR spectra of PGMA, PGMATri, PGMATri0.2TA and PGMATri3H$_3$PO$_4$, PGMATri4H$_3$PO$_4$.
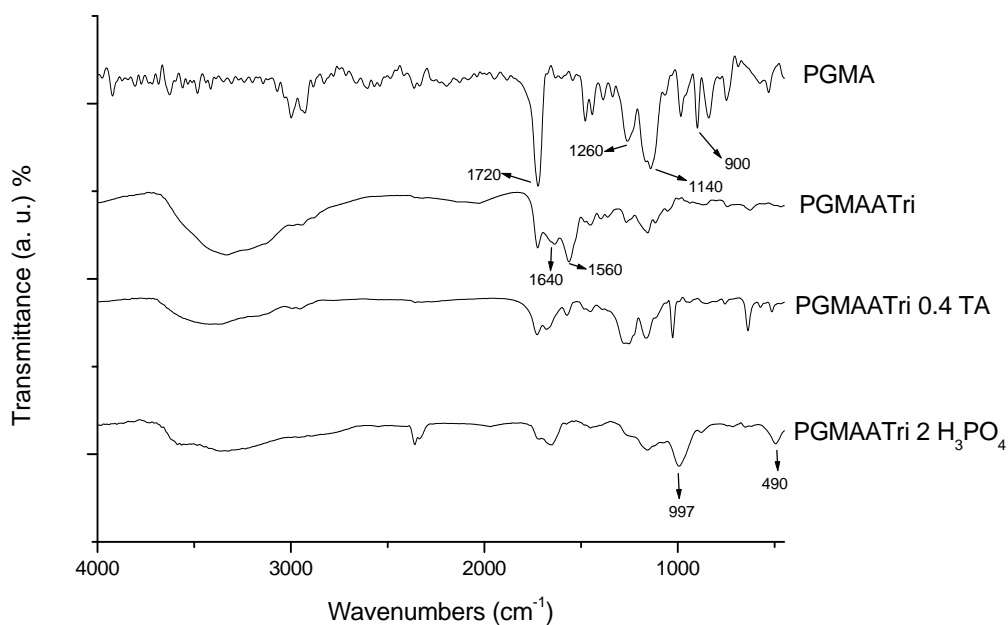
Figure 6.2 FT-IR spectra of PGMA, PGMAATri, PGMAATri0.4TA and PGMAATri2H$_3$PO$_4$.

6.1.2 FT-IR of PGMAATet

The FT-IR spectra of pristine and acid doped PGMAATet are shown in Fig. 6.3. PGMAATet exhibited a medium absorption at 1640 cm^{-1} and 1550 cm^{-1} due to amine bond and tetrazole ring vibrations (Levchik et al., 1992). The epoxy absorption peak at 900 cm^{-1} disappeared up on tetrazole functionalization. After doping the PGMAATet with H$_3$PO$_4$, two strong peaks appear near 500 cm^{-1} and 1000 cm^{-1} which are attributed to PO$_2$ bending vibration of (H$_2$PO$_4^{2-}$) and P-O symmetric stretching of H$_3$PO$_4$ (Bouchet and Siebert, 1999). The carbonyl stretching band at 1725 cm^{-1} broadens due to protonation. In addition, the disappearance of the tetrazole ring stretching at 1550 cm^{-1} as well as the formation of a broad band at 1940-1960 cm^{-1} may indicate the ring protonation (Günday et al., 2006).
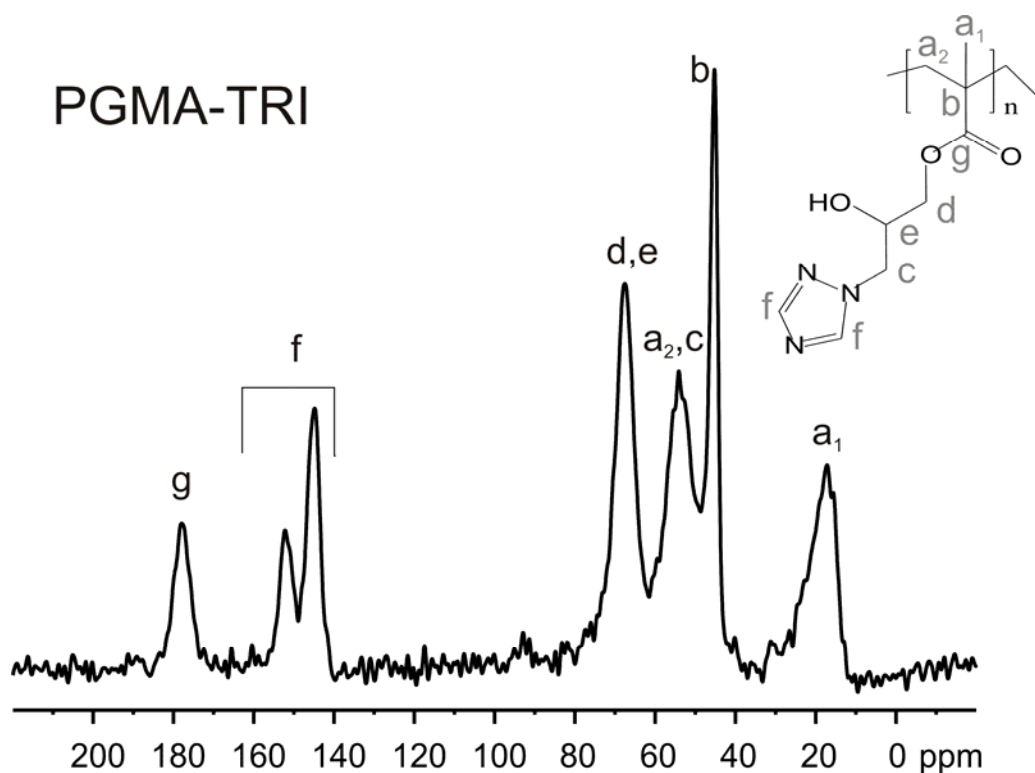

Figure 6.3 FT-IR spectra of PGMA, PGMAATet, PGMAATet3H$_3$PO$_4$ and PGMAATet4H$_3$PO$_4$.

6.2 Solid State ^{13}C CP-MAS NMR Results

6.2.1 Solid State ^{13}C CP-MAS NMR Spectra of PGMATri and PGMAATri

The solid state ^{13}C CP-MAS NMR spectra of PGMATri and PGMAATri are shown in Fig. 6.4 and Fig. 6.5, respectively. The characteristic C peaks of the azole rings are between 140-160 ppm and the peak located at around 180 ppm belongs to C of the carbonyl group. Signals corresponding to the methyl and methylene groups appear between 15-75 ppm. Resonances are similar for both samples, except those in the 140-170 ppm region. This difference in the Atri functional polymer may originate from the polymerization procedure, where the additional NH sites in the aminotriazole ring may result in some side reactions leading to inter and/or intra chain cross-linking.

Figure 6.4 The solid state ^{13}C CP-MAS NMR spectrum of PGMATri.
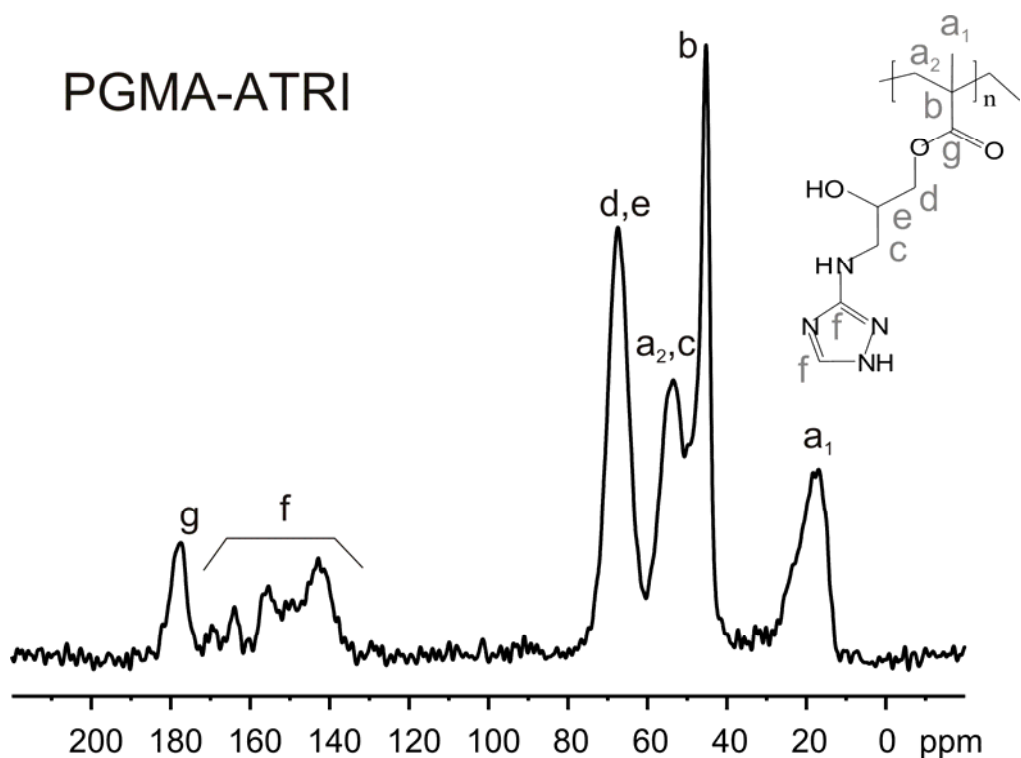
Figure 6.5 Solid state ^{13}C CP-MAS NMR spectrum of PGMAATri.

6.2.2 Solid State ^{13}C CP-MAS NMR Spectra of PGMAATet

The solid state ^{13}C CP-MAS NMR spectra of PGMAATet are shown in Fig. 6.6. The characteristic C peak of the azole ring is between 150-170 ppm and the peak located at around 180 ppm belongs to C of the carbonyl group. Signals corresponding to the methyl and methylene groups appear between 15-75 ppm.
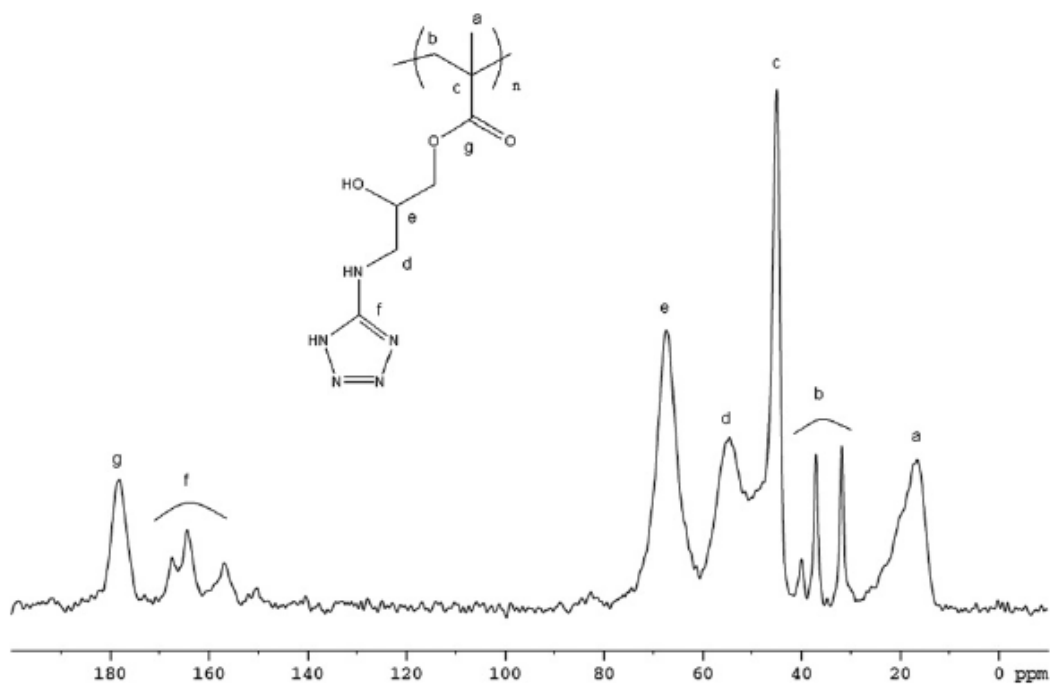
Figure 6.6 The solid state ^{13}C CP-MAS NMR spectrum of PGMAATet.

6.3 Elemental Analysis

Azole immobilization is very important for this study and elemental analysis is used to verify this reaction. The backbone of PGMA does not contain nitrogen so the nitrogen contribution into the functional polymers comes from the azole units. Nitrogen contents of the samples were used to calculate azole ratio of the functional polymers. As seen in Table 6.1 more than 78 % of the epoxide rings were opened by azole units.

**Table 6.1** Azole contents of the polymers calculated by Elemental Analysis results.

Sample	C (%)	H (%)	N (%)	Azole (%)
PGMATri	47.10	6.67	17.89	85
PGMAATri	45.09	6.24	22.05	84
PGMAATet	39.67	6.02	26.11	78

6.4 Thermogravimetry (TG) Analysis

6.4.1 TG of PGMATri and PGMAATri

It was reported that the weight loss in PGMA occurs in two steps within 200-400 ^{o}C (Nanjundan et al., 2005). Fig. 6.7 shows the thermograms of pure and doped PGMATri samples. The slight weight change until 100-150 ^{o}C can be attributed to absorbed humidity. Clearly, all the samples are thermally stable up to at least 200 ^{o}C. Above 250 ^{o}C a remarkable weight loss derives from the thermal decomposition of the polymer main chain. In PGMATri4H$_3$PO$_4$, the stepwise decomposition after 200 ^{o}C, can be attributed to water liberation due to the self-condensation of the phosphoric acid and also decomposition the polymer main chain contributes to further weight loss. Similar behavior was observed in TG analysis of pure and doped PGMAATri samples (Fig. 6.8).
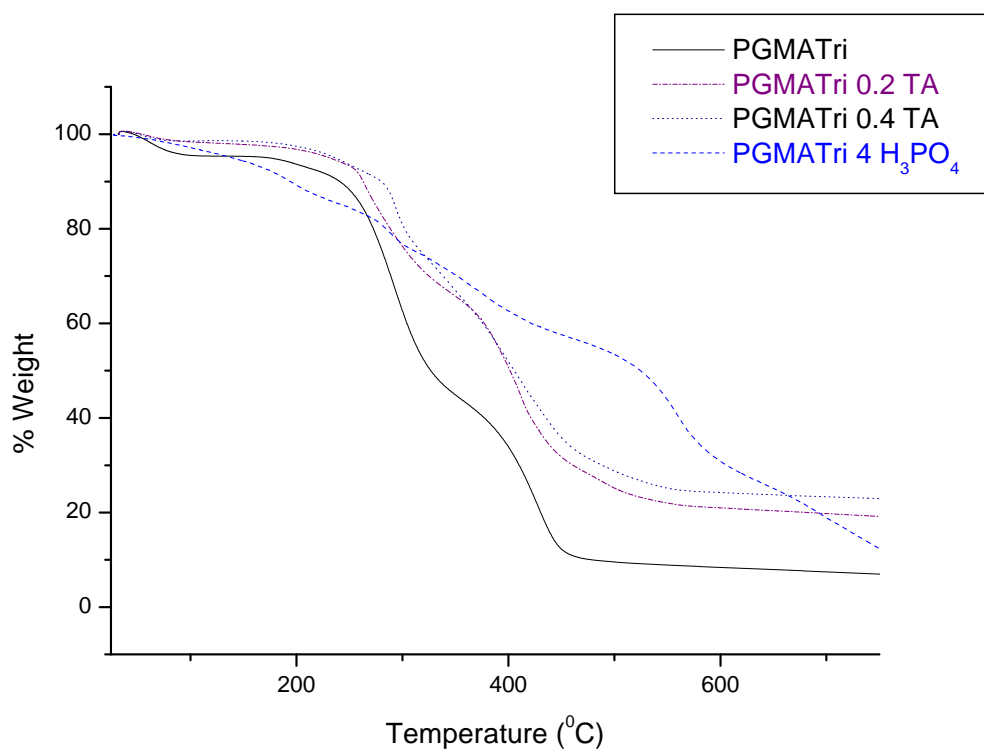
Figure 6.7 TG profiles of PGMATri, PGMATri0.2TA, PGMATri0.4TA, and PGMATri4H$_3$PO$_4$ under a N$_2$ atmosphere at a heating rate of 10 ^{0}C/min.
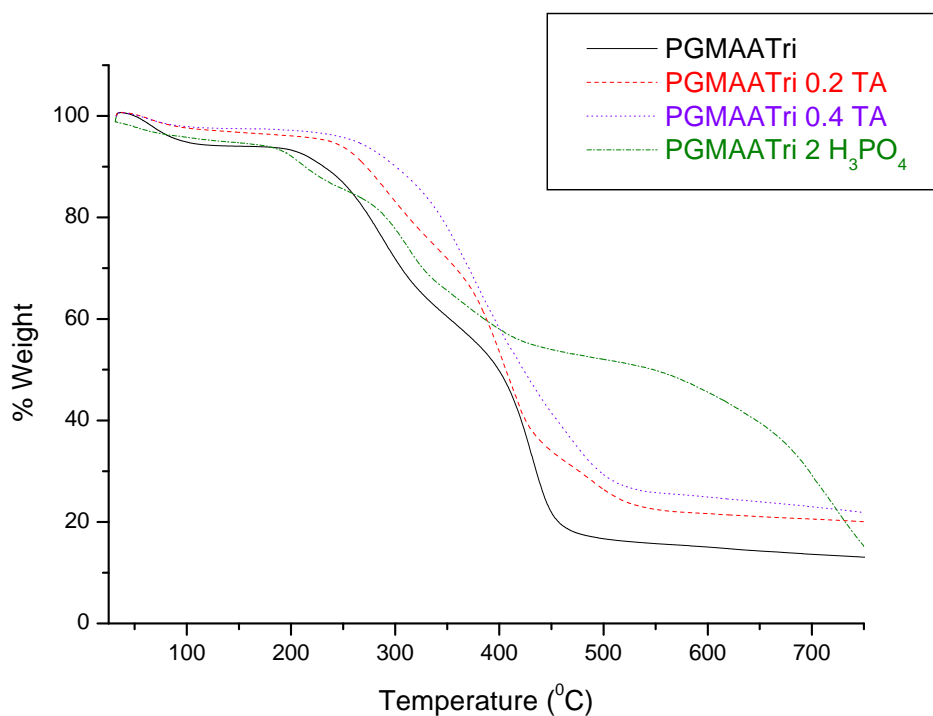
Figure 6.8 TG profiles of PGMAATri, PGMAATri0.2TA, PGMAATri0.4TA, and PGMAATri2H$_3$PO$_4$ under a N$_2$ atmosphere at a heating rate of 10 ^{0}C/min.

6.4.2 TG of PGMAATet

The thermal properties of 5-aminotetrazole was studied previously. The decomposition of 5-aminotetrazole was reported to occur above 230 ^{o}C (Lesnikovich et al., 2002). Fig. 6.9 shows the thermograms of the tetrazole functional polymer and doped sample, PGMAATet2H$_3$PO$_4$. For the PGMAATet, an elusive weight change until 230 ^{o}C may be attributed to the loss of absorbed humidity then degradation of the polymer main chain and the functional units starts. The doped samples exhibit an insignificant weight change until 200 ^{o}C. The stepwise decomposition above this temperature can be attributed to water liberation due to the self-condensation of the phosphoric acid as well as the decomposition of the polymer.
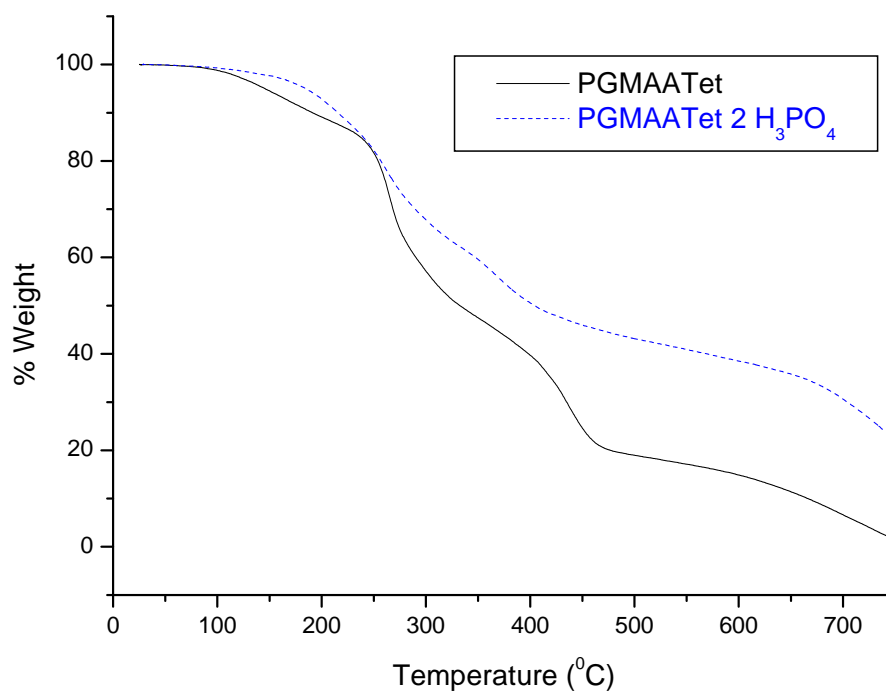
Figure 6.9 TG profiles of pure and H_3PO_4 doped PGMAATet under N_2 atmosphere at a heating rate of 10 ^{o}C/min.

6.5 DSC Measurements

6.5.1 DSC of PGMATri and PGMAATri

The glass transition temperatures (T_g) of the homopolymer (PGMA) was reported to be about 74 ^{o}C (Nanjundan et al., 2005). Fig. 6.10 shows DSC thermograms of pure and phosphoric acid doped PGMATri and PGMAATri. The T_g of PGMATri is 110 ^{o}C and that of PGMAATri is 90 ^{o}C. The curves illustrate a pronounced effect of the phosphoric acid content on the softening behavior of the materials. The T_g for PGMATri (110 ^{o}C) shifted to -35 ^{o}C for PGMATri4H$_3$PO$_4$. Similar behavior was observed for PGMAATri where T_g is shifted from 90 ^{o}C to 33 ^{o}C for PGMAATri2H$_3$PO$_4$. The presence of single glass transition shows the homogeneity of the materials.
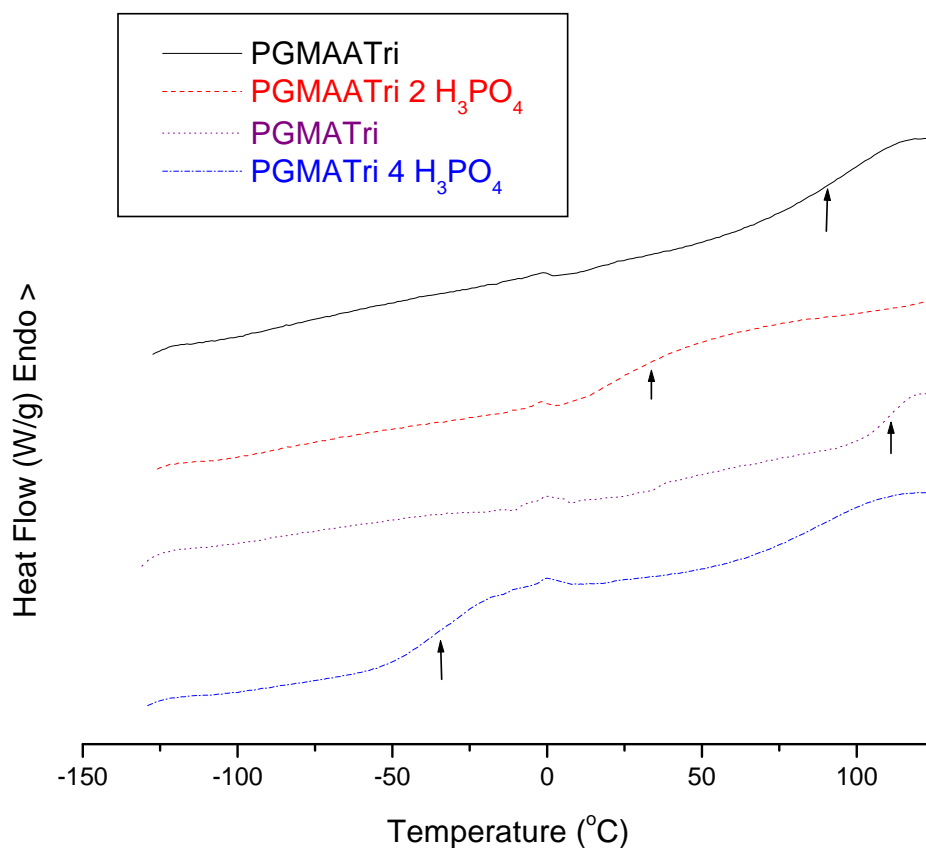
Figure 6.10 DSC thermograms of PGMAATri, PGMAATri2H$_3$PO$_4$, PGMATri and PGMATri4H$_3$PO$_4$ under a N$_2$ atmosphere at a heating rate of 10 ^{0}C/min.

6.5.2 DSC of PGMAATet

Fig. 6.11 shows the DSC thermograms of PGMAATet and phosphoric acid doped PGMAATet. The glass transition temperature of T$_g$ of the homopolymer (PGMA) was reported to be near 74 ^{o}C (Nanjundan et al., 2005). While the tetrazole functional polymer, PGMAATet has a T$_g$ of 113 ^{o}C. The Tg of PGMAATet2H$_3$PO$_4$ which was found to be 51 ^{o}C, shifted to 20 ^{o}C for PGMAATet4 H$_3$PO$_4$. Clearly, the curves indicate a pronounced effect of the phosphoric acid content on the softening behavior of the materials.
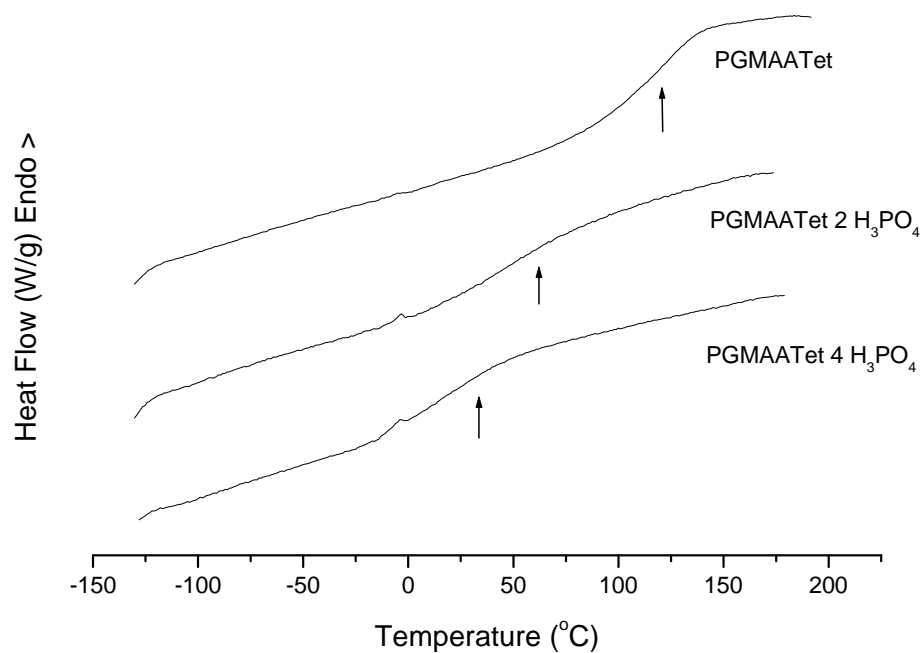
Figure 6.11 DSC traces of the pure and doped PGMAATet recorded in an inert atmosphere at a heating rate of 10 ^{o}C/min.

6.6 Proton Conductivity Studies

6.6.1 AC Conductivity Measurements

The AC conductivities, σ_{ac} (ω) of the polymers were measured at several temperatures using impedance spectroscopy. Frequency dependent AC conductivities (σ_{ac} (ω)) were measured using Eq. 1;

$$\sigma^{'}(\omega) = \sigma_{ac}(\omega) = \varepsilon^{''}(\omega)\,\omega\,\varepsilon_0 \tag{1}$$

where $\sigma^{'}$ (ω) is the real part of conductivity, $\omega = 2\pi f$ is the angular frequency, ε_0 is the vacuum permittivity ($\varepsilon_0 = 8.852 \times 10^{-14}$ F/cm), and $\varepsilon^{''}$ is the imaginary part of complex dielectric permittivity (ε^{*}).

6.6.2 DC Conductivity Measurements

The DC conductivity, σ_{dc} is derived from the log scale σ_{ac} versus F curves by linear fitting plateau regions and extrapolating to zero frequency. If the system exhibits Arrhenius behavior, the conductivity isotherm can be fitted by Arrhenius equation (Eq. 2);

$$\ln \sigma = \ln\sigma_o - E_a/kT \qquad (2)$$

where σ_o is the pre-exponential terms, E_a is the activation energy, and k is the Boltzmann constant. If the system follows VTF behavior the curved DC conductivity isotherm can be fitted by Vogel-Tamman–Fulcher-type (VTF) equation (Eq. 3);

$$\log \sigma = \log \sigma_o - E_v/[k(T-T_o)] \qquad (3)$$

where σ_o is the conductivity at infinite temperature, E_v is the Vogel activation energy and T_o is the Vogel temperature.

6.6.3 Conductivity of pure and doped PGMATri and PGMAATri

The AC and DC conductivities of pure and doped triazole functional polymers are shown in Fig. 6.12–6.20. All samples exhibit higher conductivities at high temperature and frequency. Pure polymers do not exhibit considerable proton conductivity even at high temperatures ($<10^{-6}$). In addition, there is no significant proton conductivity of triflic acid doped samples in the anhydrous state. The reason can be the aggregation triazole side groups in the host polymer which may inhibit continuous defect type conduction. Among phosphoric acid doped systems, PGMATri4H$_3$PO$_4$ showed the highest proton conductivity of ~0.01 S/cm at 150 ^{o}C in the anhydrous state. Maximum proton conductivities of all samples were summarized in Table 6.2.
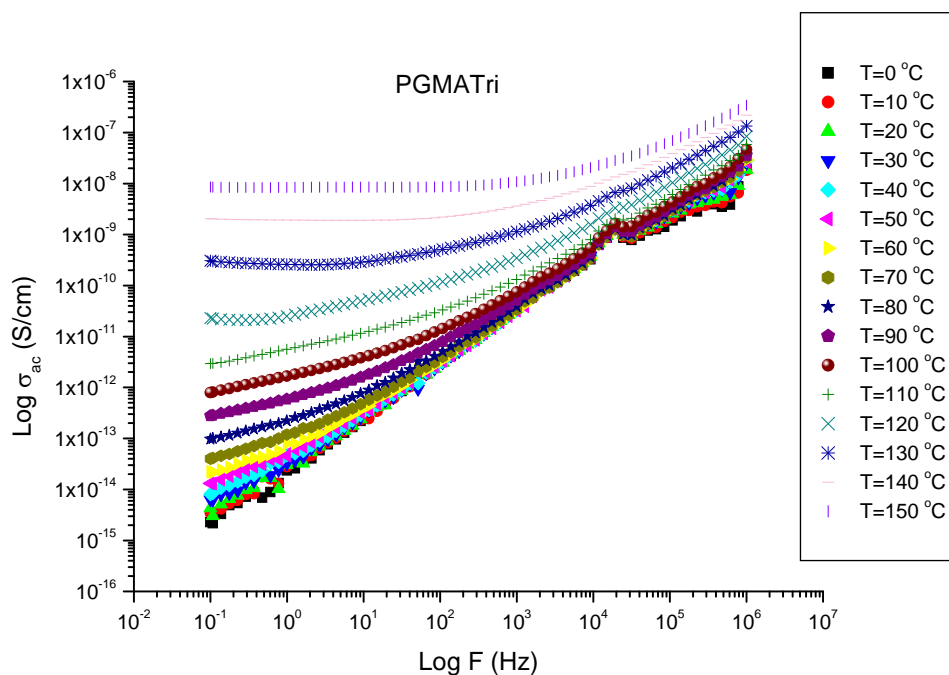
Figure 6.12 AC conductivity versus Frequency (Hz) for PGMATri at various temperatures.
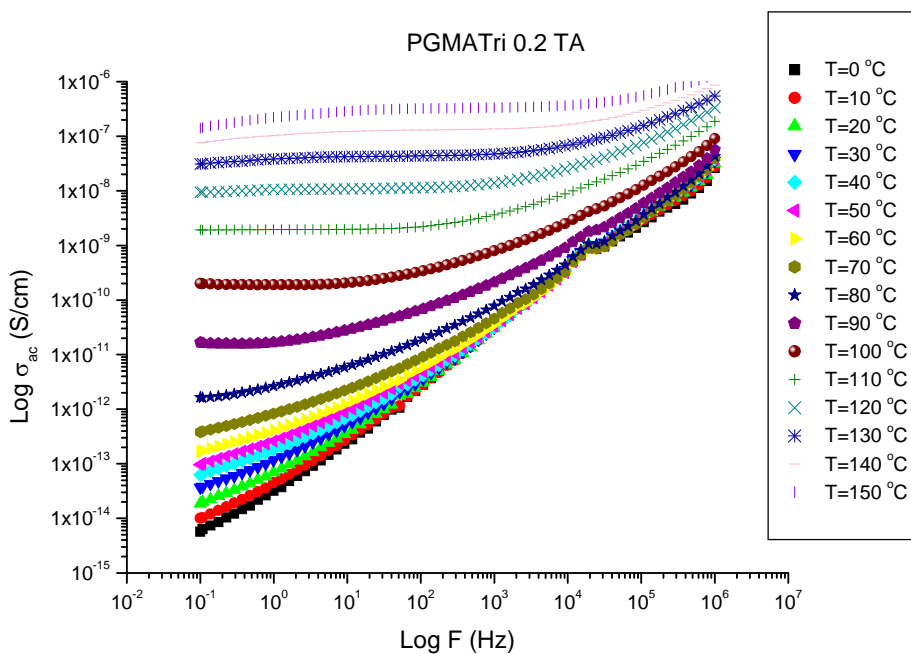
Figure 6.13 AC conductivity versus Frequency (Hz) for PGMATri0.2TA at various temperatures.
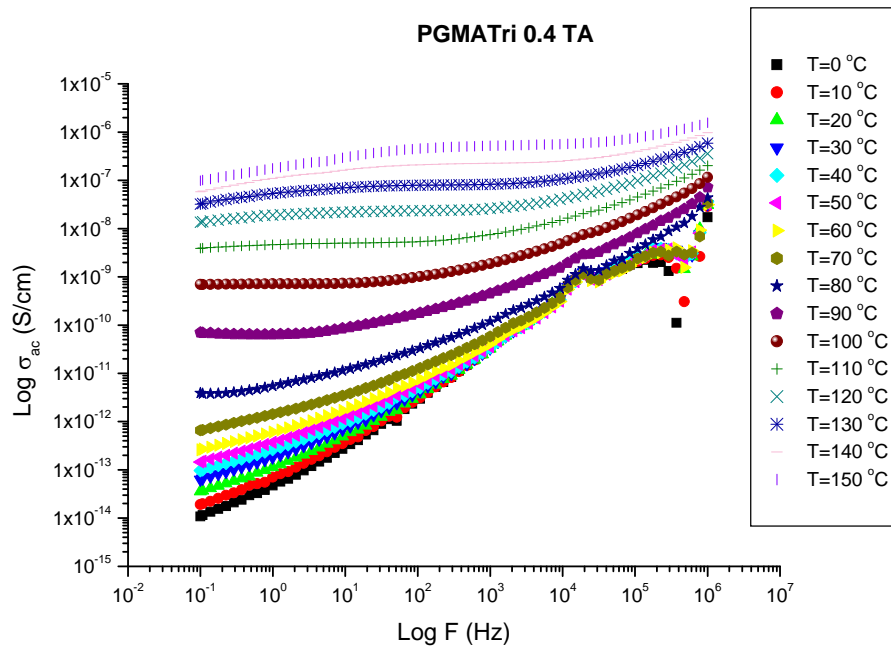
Figure 6.14 AC conductivity versus Frequency (Hz) for PGMATri0.4TA at various temperatures.

Figure 6.15 AC conductivity versus Frequency (Hz) for PGMATri4H₃PO₄ at various temperatures.

Figure 6.16 AC conductivity versus Frequency (Hz) for PGMAATri at various temperatures.

Figure 6.17 AC conductivity versus Frequency (Hz) for PGMAATri0.2TA at various temperatures.

Figure 6.18 AC conductivity versus Frequency (Hz) for PGMAATri0.4TA at various temperatures.

Figure 6.19 AC conductivity versus Frequency (Hz) for PGMAATri2H$_3$PO$_4$ at various temperatures.

Figure 6.20 DC conductivities of PGMATri4H$_3$PO$_4$, PGMAATri2H$_3$PO$_4$, PGMATri0.4TA and PGMAATri0.4TA as a function of reciprocal temperature.

6.6.4 Conductivity of pure and doped PGMAATet

The AC conductivities of phosphoric acid doped PGMAATet are shown in Fig. 6.21-6.23. All samples exhibit higher conductivities at high temperature and frequency.
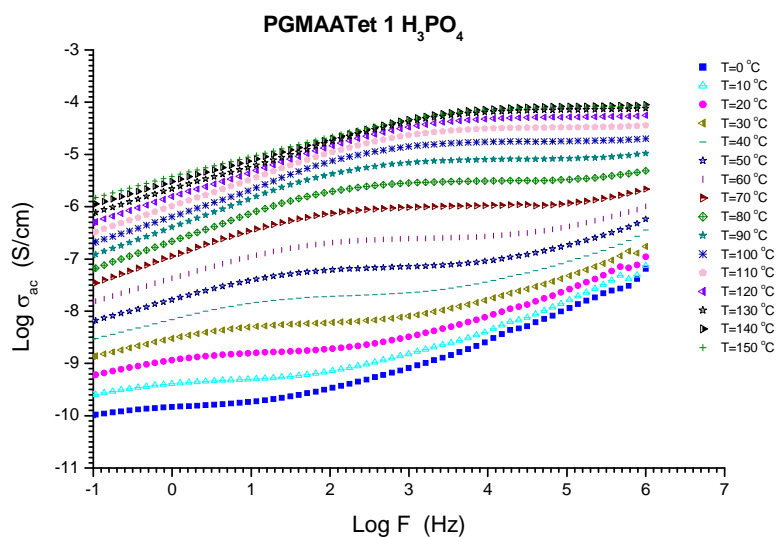
Figure 6.21 AC conductivity versus Frequency (Hz) for PGMAATet1H$_3$PO$_4$ at various temperatures.
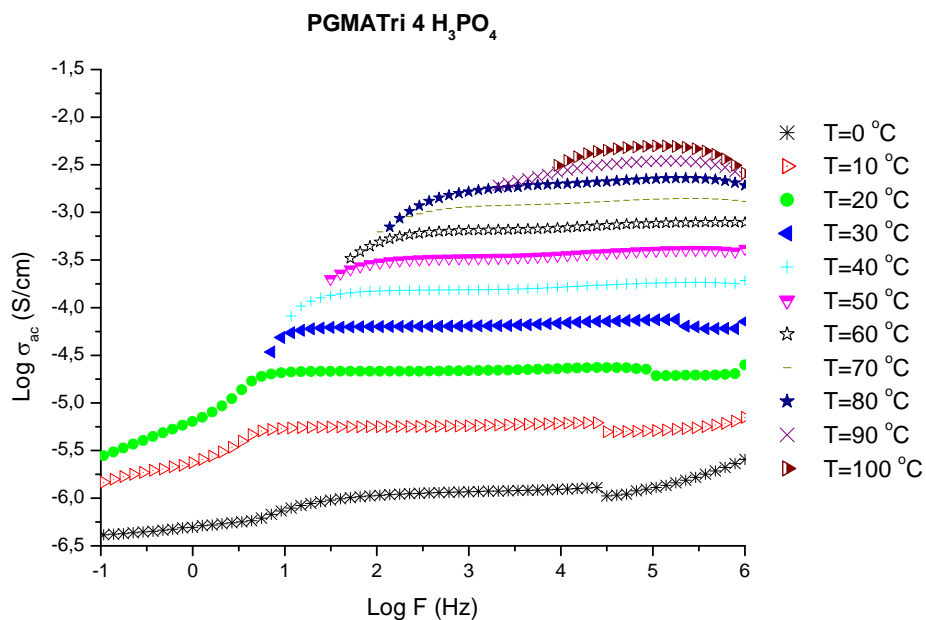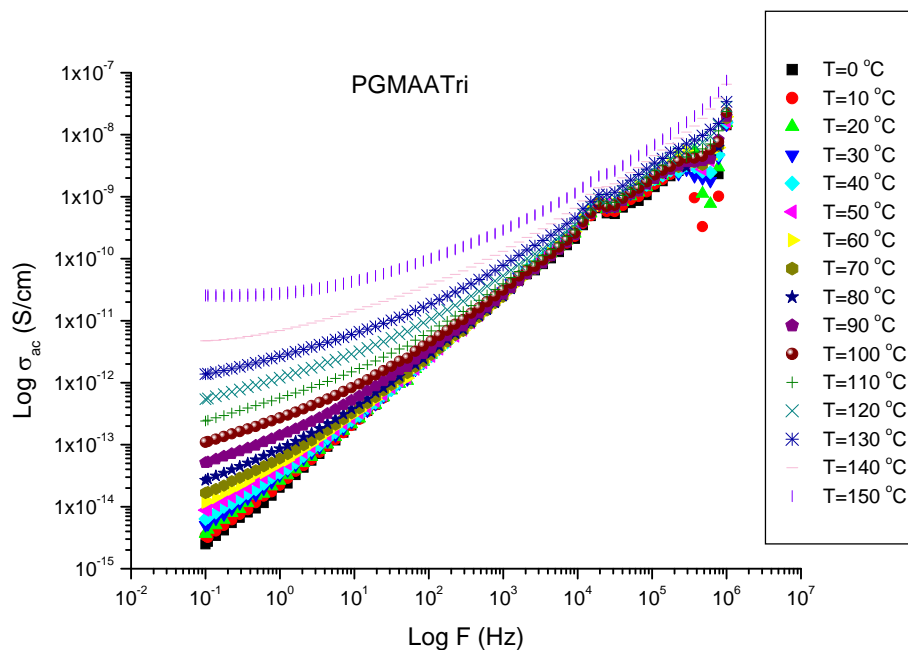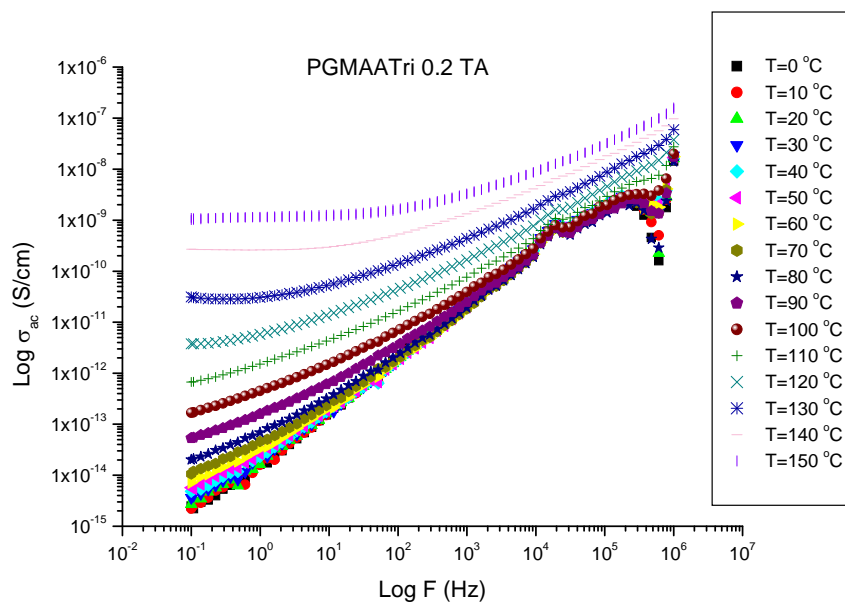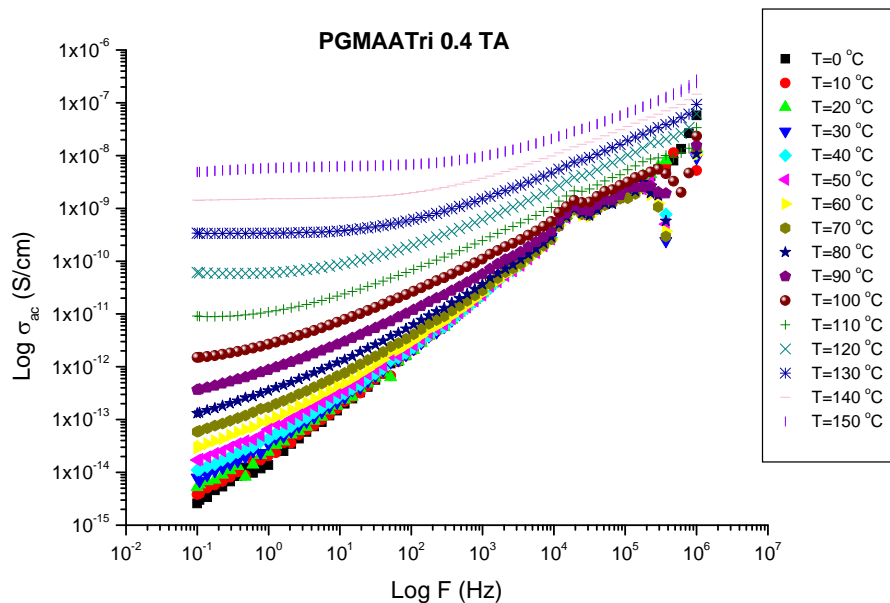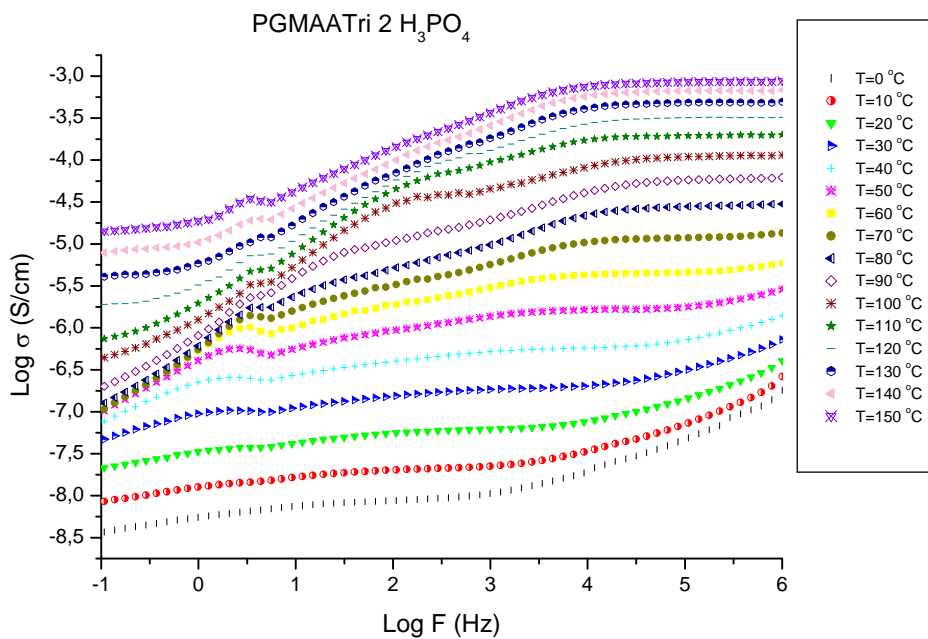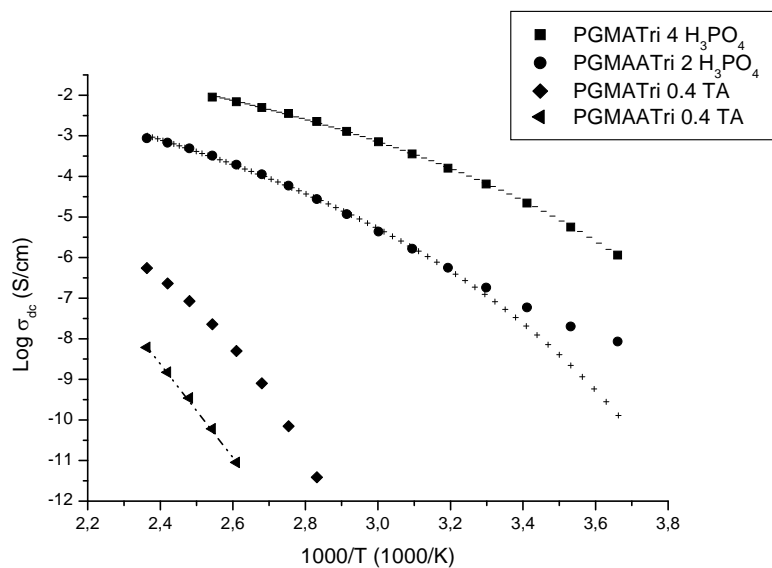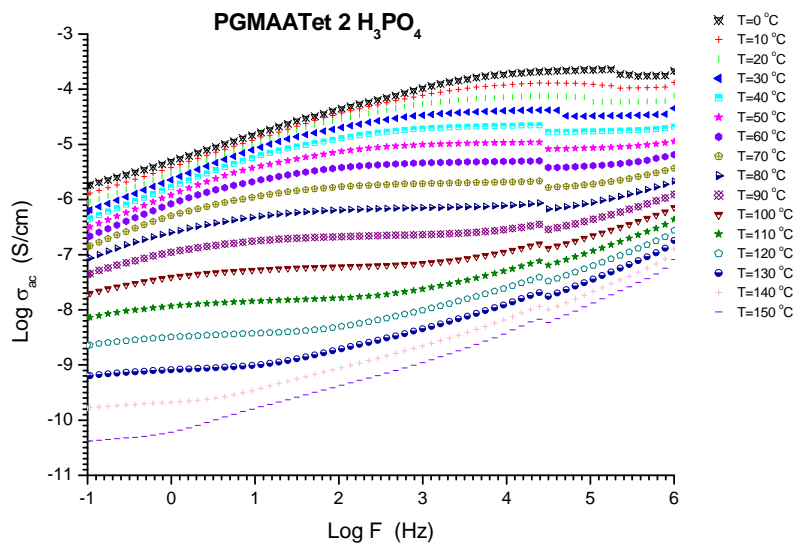
Figure 6.22 AC conductivity versus Frequency (Hz) for PGMAATet2H$_3$PO$_4$ at various temperatures.
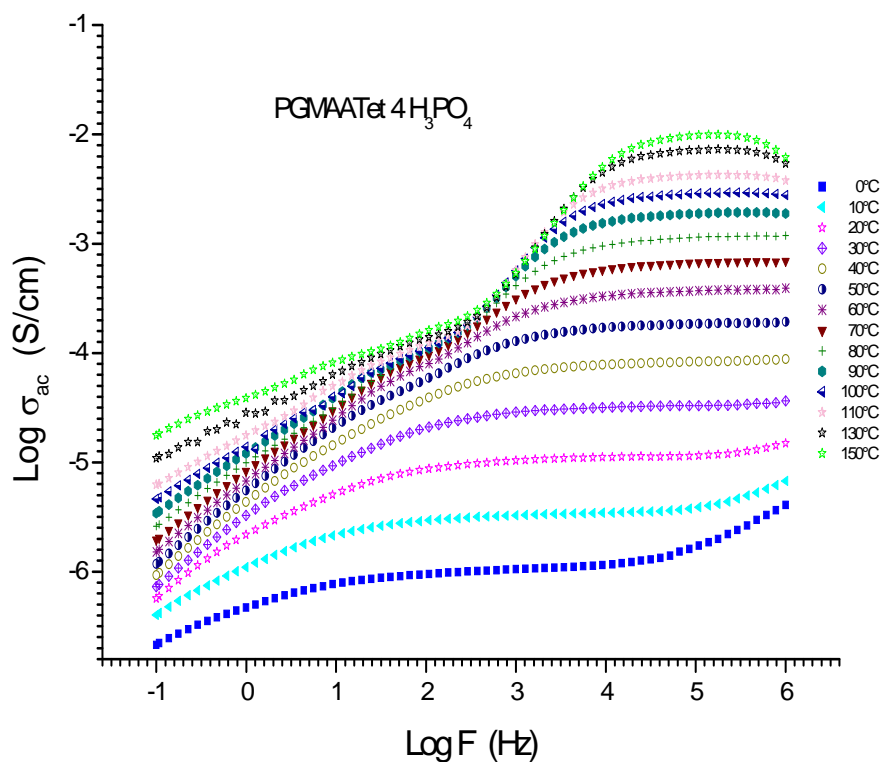
Figure 6.23 AC conductivity versus Frequency (Hz) for PGMAATet4H$_3$PO$_4$ at various temperatures.

The DC conductivities of PGMAATet samples were compared in Fig. 6.24 to determine the effect of dopant on proton conductivity. Fig. 6.24 indicates that the conductivity strongly depends on temperature and the phosphoric acid content. Generally, phosphoric acid doped systems exhibit Arrhenius behavior at lower acid contents and VTF behavior at higher acid ratio. For PGMAATet1H$_3$PO$_4$, the conductivity isotherm can be fitted by Arrhenius equation (Eq. 2). The activation energy was found to be Ea = 0.113 KJ/mol when the doping ratio x = 1. For PGMAATet2H$_3$PO$_4$ the curve slightly deviates from the Arrheniues equation and for the PGMAATet4H$_3$PO$_4$, the curved DC conductivity isotherm follows Vogel-Tamman–Fulcher-type (VTF) (Eq. 3). High accuracy of the respective VTF parameters (Table 6.3) proves the contribution of segmental relaxations to conductivity.
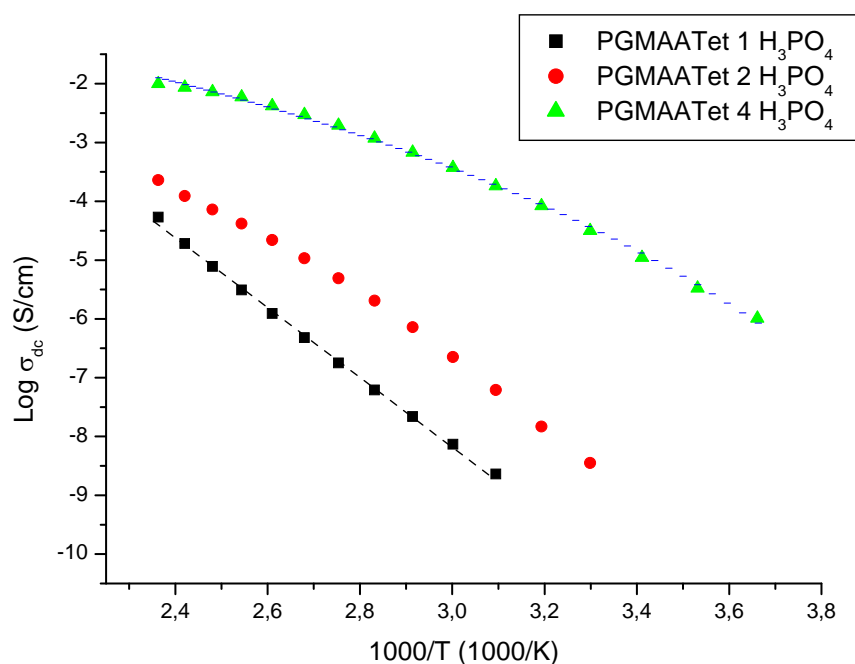
Figure 6.24 DC conductivities of PGMAATet1H$_3$PO$_4$, PGMAATet2H$_3$PO$_4$ and PGMAATet4H$_3$PO$_4$ as a function of reciprocal temperature.

There are mainly two transport mechanisms that contribute to the proton conductivity in phosphoric acid doped polymer electrolytes. The first is the structural diffusion (Grotthuss mechanism) in which the conductivity is mainly controlled by proton transport through phosphate ions, i.e. H$_4$PO$_4^+$, H$_2$PO$_4^-$ (Grotthuss proton transport). The second is the vehicle mechanism where the protons travel through the

material on a neutral or charged "vehicle". Several studies were reported about the contribution of these mechanisms on the proton conductivity of pure phosphoric acid and it was indicated that the character of conduction mechanism is mainly controlled by the structural diffusion rather than vehicle mechanism (Dippel et al., 1993).

In the PGMAATetxH_3PO_4 systems, the doping ratio is highly effective on the proton conductivity of sample which indicates that major part of proton transport is provided over the H_3PO_4 as well as over tetrazole units. Previously, the proton conductivity of acid doped PBI was reported to follow the Arrhenius law, suggesting a hopping-like conduction mechanism (He et al., 2003). In an acid doping range from 2.0 to 5.6 mol H_3PO_4, the activation energies were found to be in a range of 8 kJ/mol- 11 kJ/mol. In this novel system, the protons are transferred to neighboring units with a lower activation energy compared to PBI-H_3PO_4 systems, even at lowest acid compositions. It seems that the proton hopping from one N-H site to another contributes also to the conductivity of PGMAATetxH_3PO_4 systems as in the case of imidazole where the long range proton transfer occurs throughout the protonic defects, i.e., Him-(HimH+)-imH) (Kreuer et al., 1998). In addition, proton hopping from one N-H site to phosphate ions may also contribute to the conductivity.

From the conductivity and FTIR results, it can be concluded that the host matrix, PGMAATet includes excess phosphoric acid without significant change in the mechanical properties and conductivity occur throughout the material predominantly by Grotthuss mechanism. Maximum proton conductivities of all samples were summarized in Table 6.2. PGMAATet4H_3PO_4 showed a highest conductivity of ~1 x 10^{-2} S/cm at 150 ^{o}C in the anhydrous state.

Table 6.2 Maximum anhydrous proton conductivities of the polymer samples.

Sample	Doping acid	Acid Ratio	Conductivity	Temperature
PGMATri	-	-	3.5×10^{-7}	$150\,^{\circ}C$
	TA (CF$_3$SO$_3$H)	0.2	1.5×10^{-6}	$150\,^{\circ}C$
	TA (CF$_3$SO$_3$H)	0.4	1.6×10^{-6}	$150\,^{\circ}C$
	H$_3$PO$_4$	4	9.0×10^{-3}	$150\,^{\circ}C$
PGMAATri	-	-	7.5×10^{-8}	$150\,^{\circ}C$
	TA (CF$_3$SO$_3$H)	0.2	1.5×10^{-7}	$150\,^{\circ}C$
	TA (CF$_3$SO$_3$H)	0.4	2.5×10^{-7}	$150\,^{\circ}C$
	H$_3$PO$_4$	2	9.0×10^{-4}	$150\,^{\circ}C$
PGMAATet	H$_3$PO$_4$	1	8.5×10^{-5}	$150\,^{\circ}C$
	H$_3$PO$_4$	2	2.3×10^{-4}	$150\,^{\circ}C$
	H$_3$PO$_4$	4	1.0×10^{-2}	$150\,^{\circ}C$

Table 6.3 Maximum anhydrous proton conductivities and VTF parameters of the polymers.

Sample	Max. Conductivity (S/cm)	Log σ_0	T$_o$ (K)	E$_v$ (eV)
PGMAATri 2 H$_3$PO$_4$	9.0×10^{-4} at $150\,^{\circ}C$	0.464	198	0.154
PGMATri 4 H$_3$PO$_4$	9.0×10^{-3} at $150\,^{\circ}C$	0.793	176	0.130
PGMAATet 4 H$_3$PO$_4$	1.0×10^{-2} at $150\,^{\circ}C$	0.800	219	0.100

CHAPTER 7

CONCLUSIONS

In recent years as an alternative to perfluorinated membranes, anhydrous polymer electrolytes are produced using several polymer blends and copolymers. Heterocyclic compounds such as imidazole and triazole were used as proton source instead of water. Different composite systems were produced using heterocyclic compounds as dopant in polymers that have acidic groups. Although these systems may reach high proton conductivity, their application in fuel cells may be inefficient due to leaching out problem of the dopant. In order to improve these composite systems heterocyclic units were immobilized on the polymer backbones.

1H-1,2,4-triazole is a heterocycle that has similar structure and proton transfer mechanism with imidazole. Although it has a considerable proton conductivity of 1.2 $\times 10^{-3}$ S/cm at melting point (120 ^{o}C), direct usage of it in fuel cells is impossible due to thermal stability. In order to use its proton transfer property poly(glycidyl methacrylate) was produced by free radical polymerization of GMA and than 1H-1,2,4-triazole and 3-amino-1,2,4-triazole were immobilized by ring opening of the epoxide ring. Elemental analysis verified triazole immobilization about 85 % and the structures of the triazole functional polymers were proved by FT-IR and solid state ^{13} C CP-MAS NMR. The functional polymers were doped with phosphoric acid at several mol ratio. The proton conductivity of the materials increased with dopant concentration and the temperature. The sample PGMATri 4 H_3PO_4 showed a highest conductivity of 9.0 x 10^{-3} at 150 ^{o}C. The samples were also doped with triflic acid at low mol ratio to determine intrinsic proton conductivity of the samples. However, low conductivity was obtained for the triflic acid doped samples. This was attributed to aggregation of the triazole units in the host matrix which inhibited defect type conduction. TG analysis showed that the samples are thermally stable up to at least 200 ^{o}C. DSC results illustrated the homogeneity of the materials as well as plasticizing effect of the dopant.

As another approach for this study, 5-aminotetrazole was immobilized on PGMA and the resulting polymer was doped with phosphoric acid at several mol ratio. Elemental analysis showed tetrazole immobilization about 80 % and and the structure of the tetrazole functional polymer was proved by FT-IR and solid state ^{13}C CP-MAS NMR. TG analysis showed that the samples are thermally stable up to at least 200 ^{o}C. DSC results illustrated the homogeneity of the materials as well as plasticizing effect of the dopant. The conductivity isotherms for the phosphoric acid doped samples showed VTF behavior at higher acid compositions, indicating the contribution of polymer segmental relaxations. The conductivity is expected to occur by transport of the protons among the protogenic solvents via Grotthuss mechanism. Highest proton conductivity of 0.01 S/cm was obtained for PGMAATet4H$_3$PO$_4$ at 150 ^{o}C, in the anhydrous state.

REFERENCES

Acheson, R. M., *An Introduction to the Chemistry of Heterocyclic Compounds*, John Wiley, Canada, 1976.

Agmon N., *Chem. Phys. Lett.,* Vol. 244, pp. 456, 1995.

Agmon N., *J. Chim. Phys*. Vol. 93, pp. 1714, 1996.

Alberti G., M. Casciola, U. Costantino, M. Leonardi, *Solid State Ion.*, Vol. 14, pp. 289, 1984.

Antonucci P.L., A.S. Arico, P. Creti, E. Ramunni, V. Antonucci, *Solid State Ionics,* Vol. 125, pp. 431-437, 1999.

Bouchet R., E. Siebert, *Solid State Ionics*, Vol. 118, pp. 287-299, 1999.

Bozkurt A., M. Ise, K.D. Kreuer, W.H: Meyer, G. Wegner, *Solid State Ionics*, Vol. 125, pp. 225-233, 1999.

Bozkurt A., *Turk. J. Chem*., Vol. 26, pp. 663-668, 2002.

Bozkurt A, *Turk J Chem., Vol.* 29, pp. 117, 2005.

Bozkurt A., W.H. Meyer, *J. Polym Sci. Pol. Phys*, Vol. 39, pp. 1987-1994, 2001a.

Bozkurt A., W.H. Meyer, *Solid State Ionics*, Vol. 138, pp. 259–265, 2001b.

Bozkurt A., W.H Meyer, G. Wegner, *Journal of Power Sources*, Vol. 123, pp. 126, 2003.

Brookman, P. J.; Nicholson, J. W. in: Developments in Ionic Polymers, vol. 2; eds. A.D. Wilson and H. J. Prosser, (Elsevier Applied Science Publishers: London, 1986) pp. 269-283.

Chin D.T., H.H. Chang, *J. Appl. Electrochem.,* Vol. 19, No. 1, pp. 95, 1989.

Costamagna P., S. Srinivasan, *J. Power Sources*, Vol. 102, pp. 242-253, 2001.

Cremers C., U. Stimming, Low Temperature Fuel Cells: Development Status and Future Perspectives, , *International Union of Pure and Applied Physics*, Annex A, V- Fuel Cells, pp. 234, 2004.

Crofts A., Biophysics 354, *Biological Energy Conversion*, 1996.

Cuddeback R.B., R.C. Koeller, H.G. Drick, *J. Chem. Phys.*, Vol. 21, pp. 589, 1953.

Daniel M.F., B. Desbat, F. Cruege, O. Trinquet and J.C. Lassegues, *Solid State Ionics*, Vol. 28-30, pp. 637-641, 1988a.

Daniel M.F., B. Desbat, J.C. Lassegues, *Solid State Ionics,* Vol.28-30, pp. 632-637, 1988b.

Deng W, V. Molinero, W.A Goddard, III. *J. Am. Chem. Soc.*, Vol. 126, pp. 15644, 2004.

Dippel T., K.D. Kreuer, *Solid State Ion.,* Vol. 46, No. 1-2, pp. 3, 1991.

Dippel T., K.D. Kreuer, J.C. Lass`egues, D. Rodriguez, *Solid State Ionics,* Vol.61, No.1–3, pp. 41–46, 1993.

Donoso P., W.Gorecki, C. Berthier, F. Defendini, C. Poinsignon, MB.Armand, *Solid State Ionics,* Vol.28, No.30, pp. 969-974, 1988.

Eigen M., ed., *Ang. Chem. Intern.,* 1964.

Garcia-Viloca M, A. Gonzalez-Lafont, J.N.M Lluch,. *J. Phys. Chem. A* 1997, *101*, 3880.

Göktepe F. , A. Bozkurt, S.T. Günday, *Polymer International*, Vol. 57, pp. 133, 2008.

Greenwood N.N., A. Thompson, *J. Chem. Soc.*, pp. 3485, 1959.

Grondin J., D. Rodriguez and J. C. Lassegues, *Solid State Ionics*, Vol. 77, pp. 70-75, 1995.

Grotthuss C.J.D. v., *Ann. Chim., LVIII*, pp. 54, 1806.

Günday ST, A. Bozkurt, W.H Meyer, G. Wegner, *Journal of Polymer Science Part B: Polymer Physics*, Vol. 44, pp. 3315, 2006.

Günday ST, A. Bozkurt, N.M. Aghatabay, A.H. Baykal, *Materials Chemistry and Physics*, Vol. 105, No. 2-3, pp. 240-244, 2007.

He R., Q. Li, G. Xiao, N. J. Bjerrum, *J. Mem. Sci.,* Vol. 226, pp. 169–184, 2003.

Herz HG, K.D Kreuer, J. Maier, G. Scharfenberger, M.F.H Schuster, W.H Meyer, *Electrochim. Acta*, Vol. 48, pp. 2165, 2003.

Hirose S, T. Hatakeyama, Y. Izuta, H. Hatakeyama, *Journal of Thermal Analysis and Calorimetry,* Vol. 70, pp. 853–860, 2002.

Ianniello R., V.M. Schmidt, U. Stmming, J. Stumper, A. Wallan, *Electrochim. Acta*, Vol. 39, pp. 1863-1869, 1994.

Jang, L.K., D. Nguyen, G. Geesey, *Water Res.*, Vol. 33, pp. 2826, 1999.

Jannasch P., *Current Opinion in Colloid and Interface Science*, Vol. 8, pp. 96-102, 2003.

Karadedeli B., A. Bozkurt, A. Baykal, *Physica*, Vol. B 364, pp. 279–284, 2005.

Kawahara M., J. Morita, M. Rikukawa, K. Sanui, N. Ogata. *Electrochim. Acta*, Vol. 45, pp. 1395–1398, 2000.

Kerres J.A., *J. Mem. Sci.*, Vol. 185, pp. 3-27, 2001.

Kim J.D., I. Honma, *Solid State Ionics*, Vol. 176, pp. 979-984, 2005.

Kim J.D, T. Mori, S. Hayashi, I. Honma, *Journal of The Electrochemical Society,* Vol. 154, No. 4, pp. A290-A294, 2007.

Kreuer KD, A. Fuchs, M. Ise, M. Spaeth, J. Maier, *Electrochim. Acta,* Vol. 43, pp. 1281, 1998.

Kreuer K.D., A. Rabenau, W. Weppner, *Angew. Chem.-Int. Edit. Engl.,* Vol. 21, No. 3, pp. 208, 1982.

Kreuer, K.D., *Chemistry Materials*, Vol. 8, pp.610–641, 1996.

Kreuer K.D., *J. Membrane Sci.*, Vol. 185, pp. 29-39, 2001.

Kreuer, K.D., *Proceedings of the sixth Asian Conference on Solid State Ionic: Science and Technology*, 29 November-4 December, pp. 263, New Delhi, 1998.

Kreuer K.D., *Solid State Ion.,* Vol. 94, No.1-4, pp. 55, 1997.
.
Kreuer K.D., T. Dippel, N.G. Hainovsky, J. Maier, *Ber. Bunsen-Ges. Phys. Chem. Chem. Phys.,* Vol. 96, No. 11, pp. 1736, 1992.

Kreuer K.D., T. Dippel, W.H. Meyer, J. Maier, *Mat. Res. Soc. Symp. Proc.*, Vol. 293, pp. 273-282, 1993.

Krishnakumar V, R.J Xavier, *Spectrochimica Acta Part A*, Vol. 60, pp. 709–714, 2004.

Lassegues J.C., B. Desbat, O. Trinquet, F. Cruege, C. Poinsignon, *Solid State Ion.*, Vol. 35, No.1-2, pp. 17, 1989.

Lassegues J.C., J. Grondin, M. Hernandez, B.Maree, *Solid State Ionics,* Vol. 145, No. 1-4, pp. 37–45, 2001.

Lassegues J.C., *Proton Conductors, Solids Membranes, and Gels-Materials and Gels-Materials and Devices*, ed. P.Colomban, Cambridge University Press, Cambridge, pp. 311-328, 1992.

Lesnikovich AI, O.A Ivashkevich, S.V Levchik, A.I Balabanovich, P.N Gaponik, A.A Kulak, *Thermochimica Acta*, Vol. 388, pp. 233-251, 2002.

Levchik SV, G.A Ivashkcvich, A.I Balabanovich, A.I Lesnikovich, P.N Gaponik, L. Costa, *Thermochimica Acta*, Vol. 207, pp. 115-130, 1992.

Li S., Z. Zhou, Y. Zhang, M. Liu, *Chem. Mater.,* Vol. 17, pp. 5884-5886, 2005.

Li Q. , H.A. Hjuler, N.J. Bjerrum, *Electrochim. Acta*, Vol. 45, pp. 4219-, 2000.

Li Q., H.A. Hjuler, N.J. Bjerrum*, J. Appl. Electrochem.,* Vol. 31, pp. 773-779, 2001.

Li Q. F., R.H. He, J.A. Gao, J.O. Jensen, N.J. Bjerrum, *J. Electrochem. Soc*., Vol. 150, No. 12, pp. A1599-, 2003.

Ma Y., *The Fundamental Studies of Polybenzimidazole/Phosphoric acid Polymer Elevtrolyte for Fuel Cells*, Ph. D Thesis, Case Western Reverse University, 2004.

Miyake N., J.S. Wainright, R.F. Savinell, *J. Electrochem. Soc.*, Vol. 148, pp. A898-A904, 2001.

Moore B.D, D.C Sherrington, A. Zitsmanis, *J. Mater. Chem.,* Vol. 2, pp. 1231-, 1992.

Motupally S., A.J. Becker, J.W. Weidner, *J. Electrochem. Soc.*, Vol. 147, No. 9, pp. 3171-3177, 2000.

Munson R.A., *J. Phys. Chem.*, Vol. 68, No.11, pp. 3374–3377, 1964.

Münch, W., K.D. Kreuer, W. Silvestri, J. Maier, G. Seifert, *Solid State Ionics*, Vol. 145, pp. 437–443, 2001.

Nanjundan S, C.S Unnithan, C.S.J Selvamalar, A. Penlidis, *React. Funct. Polym.*, Vol. 62, pp. 11-, 2005.

Noda A, M. Susan, H.B. Abu, K. Kudo, S. Mitsushima, K. Hayamizu, M.J Watanabe, *Phys. Chem. B,* Vol. 107, pp. 4024, 2003.

Persson J.C., P. Jannasch, *Macromolecules*, Vol. 38, No. 8, pp. 3283-3289, 2005.

Persson J.C., K. Josefsson, P.Jannasch, *Polymer*, Vol. 47, pp. 991–998, 2006.

Petty-Week S., J.J. Zupancic, J.R. Swedo, *Solid State Ionics*, Vol. 31, pp. 117-125, 1988.

Polak A.J., S. Petty-Weeks and A.J.Beuhler, *Sensors and Actuators*, Vol. 9, pp. 1-7, 1986.

Przyluski J. and W. Wieczorek, *Synthetic Metals,* Vol. 45, pp. 323-333, 1991.

Przyluski J., A. Dabrawska, S. Stys, W Wieczorec, *Solid State Ionics*, Vol. 60, pp. 141-146, 1993.

Przyluski J., W. Wieczorec, S. Glowinkowski, *Electrochim. Acta*, Vol. 37, pp. 1733-1735, 1992.

Pu H., Q. Liu, G. Liu, *Journal of Membrane Science*, Vol. 241, pp. 169–175, 2004.

Pu H., W.H. Meyer, G. Wegner, *J. Polym. Sci. Polym. Phys.,* Vol. 40, pp. 663–669, 2002.

Pu H., W.H. Meyer, G. Wegner, *Macromol. Chem. Phys.*, Vol. 202, No. 9, pp. 1478–1482, 2001.

Pu H, S. Ye, React. Funct. Polym., Vol. 66, pp. 856-, 2006.

Qingfeng L., H.A. Hjuler, N. J. Bjerrum, *J. Appl. Electrochem.,* Vol. 31, pp. 773-779, 2001.

Rikukawa M., K. Sanui, *Prog. Polym. Sci.*, Vol. 25, pp. 1463-1502, 2000.

Rodriguez D., C. Jegat, O. Trinquet, J grondin, J. C. Lassegues, *Solid State Ionics*, Vol. 61, pp. 195-202, 1993.

Rousseau F., M. Popall, H. Schmidt, C. Poinsignon, M. Armand, *Proc.2nd Int. Symp. Polymeric Electrolytes*, Siena, pp. 325-338, 1989.

Samms S.R., S. Wasmus, R.F. Savinell, *J. Electrochem. Soc.*, Vol. 143, pp. 1225–1232, 1996.

Sari H., A.K. Covington, *Journal of Chemical and Engineering Data*, Vol. 50, No. 4, pp. 1425, 2005.

Scharfenberger G, W.H Meyer, G. Wegner, M. Schuster, K.D Kreuer, J. Maier*, Fuel Cells,* Vol. 3-4, pp. 237–250, 2006.

Schoolman D., O. Trinquet, J.C. Lassegues, *Electrochim. Acta*, Vol. 37, pp. 1619-1621, 1992.

Schuster M.F.H., W.H. Meyer, *Annu. Rev. Mater. Res.*, Vol. 33, pp. 233-261, 2003.

Schuster M.F.H, W.H Meyer, G. Wegner, H.G. Herz, M. Ise, M. Schuster, K.D. Kreuer, J. Maier, *Solid State Ionics,* Vol. 145, pp. 85, 2001.

Slade R.C.T., A. Hardwick, and e. al., *Solid State Ion.,* Vol. 9-10, pp. 1091, 1983.

Smitha B., S. Sridhar, A.A. Khan, *J. Mem. Sci.*, Vol. 259, pp. 10-26, 2005.

Tanaka R., H. Yamamoto, A. Shono, K. Kubo, M. Sakurai, *Electrochim. Acta*, Vol. 45, No. 8–9, pp. 1385–1389, 2000.

Tanaka R., H. Yamamoto, S. Kawamura, T. Iwase, *Electrochim. Acta*, Vol. 40, pp. 2421–2429, 1995.

Wainright J.S., Wang J.T., Weng D., Savinell R.F., Litt M., *J. Electrochem. Soc.,* Vol. 142, pp. L121–L123, 1995.

Wang J.T., J.S. Wainright, R.F. Savinell, M. Litt, *J. Appl. Electrochem.*, Vol. 26, pp. 751–756, 1996a.

Wang J.T., R.F. Savinell, J. Wainright, M. Litt, H. Yu, *Electrochim. Acta,* Vol. 41, pp. 193–197, 1996b.

Watkins DS. In: Blomen LJMJ, Mugerwa MN, editors. *Fuel cell systems,* New York: Plenum Press, pp. 493, 1993.

Weng D., J.S. Wainright, U. Landau, R.F. Savinell,. *J. Electrochem. Soc.*, Vol. 143, pp. 1260–1263, 1996.

Wieczorec W., Z. Florjanczyk, J.R. Stevens, *Electrochim. Acta*, Vol. 40, pp. 2327-2330, 1995.

Woudenberg R.C., O. Yavuzcetin, M.T. Tuominen, E.B. Coughlin, *Solid State Ionics,* Vol. 178, pp. 1135-1141, 2007.

Yamada M., I. Honma, *Angew Chem*, Int Ed., Vol. 43, pp. 3688, 2004a.

Yamada M., I. Honma, *Electrochimica Acta*, Vol. 48, pp. 2411, 2003.

Yamada M., I. Honma, *Electrochimica Acta*, Vol. 50, pp. 2837–2841, 2005a.

Yamada M., I. Honma, *Polymer* , Vol. 45, pp. 8349-8354, 2004b.

Yamada M., I. Honma, *Polymer*, Vol. 46, pp.2986, 2005b.

Yang C, P. Costamagna, S. Srinivasan, J. Benziger, A.B Bocarsly, *J. Power Sources*, Vol. 103, pp. 1-9, 2001.

Yeager H.J, A. Eisenberg, in: Perfluorinated Ionomer Membranes; eds. A. Eisenberg and H. L. Yeager, *ACS Symp.* Ser. No.180, (American Chemical Society: Washington,DC, 1982) pp. 1-6, 41-63.

Zawodzinski T.A, C. Derouin, S. Radzinski, R.J. Sherman, V.T. Smith, T.E. Springer, S. Gottesfeld, *J. Electrochem Soc*, Vol. 140, pp. 1-7, 1993.

Zhou Z., S.W. Li, Y.L. Zhang, M.L. Liu, W. Li, *Journal of the American Chemical Society* , Vol. 127, No. 31, pp. 10824, 2005.

Zhou Z., R. Liu, J.H. Wang, S.W. Li, M.L. Liu, J.L. Bredas, *Journal of Physical Chemistry A*, Vol. 110, No. 7, pp. 2322, 2006.